Geochemistry, Geophysics, Geosystems

RESEARCH ARTICLE
10.1029/2021GC009918

Modeling the Viscosity of Anhydrous and Hydrous Volcanic Melts

D. Langhammer[1], D. Di Genova[1], and G. Steinle-Neumann[1]

[1]Bayerisches Geoinstitut, Universität Bayreuth, Bayreuth, Germany

Key Points:

- We provide a temperature- and water-dependent viscosity model for volcanic melts that performs better or comparable to literature models
- Anhydrous data are fit to explore the constant infinite temperature viscosity. Polymerized melts skew results toward lower values
- Differential scanning calorimetry data enable extrapolation of viscosity to any temperature using a constant value at infinite temperature

Supporting Information:

Supporting Information may be found in the online version of this article.

Correspondence to:

D. Langhammer,
dominic.langhammer@uni-bayreuth.de

Citation:

Langhammer, D., Di Genova, D., & Steinle-Neumann, G. (2021). Modeling the viscosity of anhydrous and hydrous volcanic melts. *Geochemistry, Geophysics, Geosystems*, *22*, e2021GC009918. https://doi.org/10.1029/2021GC009918

Received 20 MAY 2021
Accepted 5 AUG 2021

Abstract The viscosity of volcanic melts is a dominant factor in controlling the fluid dynamics of magmas and thereby eruption style. It can vary by several orders of magnitude, depending on temperature, chemical composition, and water content. The experimentally accessible temperature range is restricted by melt crystallization and gas exsolution. Therefore, modeling viscosity as a function of temperature and water content is central to physical volcanology. We present a model that describes these dependencies by combining a physically motivated equation for temperature dependence of viscosity and a glass transition temperature (T_g) model for the effects of water. The equation uses the viscosity at infinite temperature η_∞, T_g, and the steepness factor m as fitting parameters. We investigate the effect of leaving η_∞ free as a parameter and fixing its value, by fitting anhydrous viscosity data of 45 volcanic melts using the temperature dependent model. Both approaches describe experimental data well. Using a constant η_∞ therefore provides a viable route for extrapolating viscosity from data restricted to small temperature intervals. Our model describes hydrous data over a wide compositional range of terrestrial magmas (26 data sets) with comparable or better quality than literature fits. With η_∞ constrained, we finally apply our model to viscosities derived by differential scanning calorimetry and find—by comparing to viscometry based data and models—that this approach can be used to reliably describe the dependence of viscosity on temperature and water content. This introduces important implications for modeling the effects of nanostructure formation on viscosity.

Plain Language Summary How violently a volcano erupts strongly depends on the viscosity of the ascending magma. Temperature and the amount of dissolved water in the magma significantly impact viscosity. Therefore, models that predict it as a function of these parameters are of great interest and can be calibrated by measured data. We find a model that performs comparably to or better than other published ones. One model parameter describes the viscosity at infinite temperature; we investigate whether this is a constant value for all melts, and find this to be a justifiable assumption that leads to accurate predictions. Finally, we explore the possibility of deriving viscosity via differential scanning calorimetry (DSC). This approach avoids or significantly reduces melt crystallization which is a possible consequence of using more common measurement methods. By combining the constant value for the infinite temperature viscosity with DSC-derived data, our model can accurately predict viscosity at any relevant temperature.

1. Introduction

The shear viscosity (η) of naturally occurring aluminosilicate (i.e., volcanic) melts controls their transport at depth, the way they evolve to a crystal- and/or bubble-bearing system (i.e., magma) and, therefore, multiphase η of magma. The viscosity of a magma also regulates its ascent rate to the Earth's surface, the rheological response to deformation, the degassing and outgassing regime, and determines the style of volcanic eruptions (Cassidy et al., 2018; Colucci & Papale, 2021; Di Genova, Kolzenburg, et al., 2017; Dingwell, 1996; Gonnermann & Manga, 2007; Papale, 1999).

Consequently, the study of magma viscosity remains a central objective in physical volcanology as its parametrization feeds numerical models of volcanic eruptions (Gonnermann & Manga, 2013; Papale, 1999), pyroclastic density current scenarios (Ongaro et al., 2008), and ash-cloud transport (Mastin et al., 2009) that are used for operational forecasting of eruption evolution and planning of emergency response and evacuation (Marzocchi et al., 2012). The viscosity of magmas spans 10^{-3} – 10^{13} Pa s and is controlled by temperature (T), melt composition (x), micro and nanocrystals (Φ_c), and bubble (Φ_b) volume fraction

(Bagdassarov & Dingwell, 1992; Caricchi et al., 2007; Chevrel et al., 2015; Cordonnier et al., 2009; Costa et al., 2009; Davì et al., 2009; Dingwell et al., 1996, 2004; Di Genvova, Brooker, et al., 2020; Di Genova, Kolzenburg, et al., 2017; Di Genova, Romano, Alletti, et al., 2014; Di Genova, Zandona, & Deubener, 2020; Dobson et al., 1996; Giordano et al., 2009; Hess et al., 2001; Ishibashi & Sato, 2007; Kolzenburg et al., 2018; Lejeune et al., 1999; Liebske et al., 2003, 2005; Manga et al., 1998; Misiti et al., 2011; Mueller et al., 2010; Norton & Pinkerton, 1997; Pistone et al., 2012; Richet et al., 1996; Robert et al., 2013; Romano et al., 2003; Sehlke et al., 2014; Stabile et al., 2016; Stagno et al., 2018; Stein & Spera, 2002; Vetere et al., 2008, 2013; Vona et al., 2011, 2016, 2017; Whittington et al., 2001). Oxygen fugacity is a chemical variable that can affect volcanic melt and magma viscosity in different ways (e.g., Bouhifd et al., 2004; Kolzenburg et al., 2018; Sato, 2005; Stabile et al., 2021; Vetere et al., 2008): it determines the Fe^{3+}/Fe^{2+} ratio in the melt, where the latter acts as a network modifier and the former can act as a network former. This results in opposite effects on melt viscosity; with increasing Fe^{3+} content, the melt viscosity increases. The Fe^{3+}/Fe^{2+} ratio affects the viscosity in polymerized melts (e.g., rhyolites; Stabile et al., 2021) more strongly than in depolymerized melts (e.g., basalts; Kolzenburg et al., 2018). However, the Fe^{3+}/Fe^{2+} ratio also shifts phase equilibria (Hamilton et al., 1964; Markl et al., 2010; Wilke, 2005), influencing the melt crystallization path (Toplis & Carroll, 1995) and rheological evolution (Bouhifd et al., 2004; Kolzenburg et al., 2018; Sato, 2005). Moreover, it has been demonstrated that changing the dissolved iron content in melts is responsible for iron nanolite formation which, in turn, affects melt viscosity (Di Genova, Kolzenburg, et al., 2017). The knowledge of melt viscosity $\eta(T,x)$ represents the foundation on which multiphase descriptions of magma viscosity $\eta(T,x,\Phi_c,\Phi_b)$ are developed (Llewellin & Manga, 2005; Mader et al., 2013; Phan-Thien & Pham, 1997; Pistone et al., 2016; Truby et al., 2015). Therefore, extensive literature provides empirical parametrizations of $\eta(T,x)$ for an ever expanding compositional space (Baker, 1996; Bottinga & Weill, 1972; Duan, 2014; Giordano & Dingwell, 2003a; Giordano et al., 2006, 2009; Hess & Dingwell, 1996; Hui & Zhang, 2007; Romine & Whittington, 2015; Shaw, 1972).

A combination of concentric cylinder and falling sphere viscometry is employed to measure melt η above the liquidus T in the low-η/high-T regime (Lη, 10^{-3} Pa s < η < 10^5 Pa s), while micropenetration and parallel plate techniques are routinely used in the high-η/low-T regime (Hη, 10^8 Pa s < η < 10^{13} Pa s) around the glass transition temperature T_g at which

$$\eta(T_g) = 10^{12}\,\text{Pa s}. \tag{1}$$

Due to experimental inaccessibility of $\eta < 10^{-3}$ Pa s and rapid crystallization or exsolution of volatiles for 10^5 Pa s < η < 10^8 Pa s on the timescale of measurements, interpolation between the Hη and Lη regimes is required. This is especially critical when the Lη and Hη intervals of experiments are reduced as a result of nanostructure formation, primarily nanocrystals and melt demixing, which can lead to a significant increase in η (Di Genova, Brooker, et al., 2020; Di Genova, Kolzenburg, et al., 2017; Di Genova, Zandona, & Deubener, 2020; Liebske et al., 2003). These restrictions on the Hη range accessible to micropenetration and parallel plate experiments can lead to the virtual absence of data near T_g (Al-Mukadam et al., 2020; Chevrel et al., 2013; Dingwell et al., 2004).

Here, we present a new fitting approach for η of volcanic melts motivated by physically based equations that describe the temperature dependence of viscosity (Mauro et al., 2009) and water dependence of T_g (Schneider et al., 1997). This represents one of the first attempts to combine physically based equations in order to provide a single formulation for the viscosity of volcanic melts as a function of temperature and water over a large chemical space, with a set of 1,603 η data points, containing both multicomponent dry and hydrous systems as indicated in the total alkali-silica (TAS) diagram (Le Bas et al., 1986, Figure 1). To characterize the behavior of anhydrous melts in a systematic way, we order them according to the chemical parameter SM, which is a proxy of the degree of structural polymerization (Giordano & Dingwell, 2003a). We calculate SM as

$$\text{SM} = x_{\text{FeO}} + x_{\text{MgO}} + x_{\text{MnO}} + x_{\text{CaO}} + x_{\text{Na}_2\text{O}} + x_{\text{K}_2\text{O}}, \tag{2}$$

with x in mol%; for compositions that only report total iron, we distribute it equally between FeO and Fe_2O_3 with an adjustment factor of 1.11 (reflecting the higher molar weight of Fe_2O_3) in terms of wt% before conversion.

First we investigate the fit of η for anhydrous samples using a model developed by Mauro et al. (2009) for technical glasses. We discuss the connection between Arrhenian behavior of volcanic melt η and the degree of structural polymerization (SM) as well as the hypothesis of a common viscosity value at infinite T (η_∞) for glass-forming melts. We do so by significantly expanding previous chemical and experimental data sets of melt viscosity data (Russell et al., 2003). For a given silicate melt, the addition of H_2O can reduce the viscosity in the Hη regime by several orders of magnitude (e.g. Richet et al., 1996). We ignore the pressure effect on melt viscosity at fixed water content at shallow conditions typical of volcanic systems (Giordano et al., 2008; Hui & Zhang, 2007; Persikov, 1998; Zhang et al., 2003), but our model implicitly accounts for the pressure effect by varying the water content. Many studies (e.g., Dingwell et al., 1998b; Giordano et al., 2009; Misiti et al., 2011; Robert et al., 2015; Vetere et al., 2006; Whittington et al., 2009) have modeled the influence of H_2O on η by various differing empirical expressions. We apply a single formulation for water dependence of η and compare our results to published models from the literature. We show that our physically based viscosity equation can perform comparably or better than empirical formulations in the literature. Furthermore, we compare results of our fit with predictions of general chemical models (Duan, 2014; Giordano et al., 2008; Hui & Zhang, 2007). Finally, we apply our model to describe η of hydrous volcanic melts based on differential scanning calorimetry (DSC) measurements, which minimizes or avoids nanocrystallization that can occur during standard viscosity measurement around T_g (Di Genova, Zandona, & Deubener, 2020). We implement our model with a constant $\log \eta_\infty$ and show that the combination of our fitting approach with DSC data allows both the accurate prediction of high-temperature η and the quantification of the effect nanocrystal formation has on melt viscosity around T_g.

2. Approaches for Modeling Silicate Melt Viscosity

2.1. Viscosity Models for Anhydrous Systems

The most popular parametrization to describe the viscosity of volcanic melts is the empirical VFT equation named after Vogel (Vogel, 1921), Fulcher (Fulcher, 1925), and Tammann (Tammann & Hesse, 1926). It has been used to fit isochemical η data (e.g. Richet et al., 1996; Whittington et al., 2001) and takes the form

$$\log \eta = A_{\mathrm{VFT}} + \frac{B_{\mathrm{VFT}}}{T - C_{\mathrm{VFT}}}. \tag{3}$$

A_{VFT}, B_{VFT}, C_{VFT} are fitting parameters, where $A_{\mathrm{VFT}} = \log \eta_\infty$. The VFT equation has been successful in modeling the viscosity of silicate melts. Due to its empirical nature, assigning physical meaning to the fitting parameters B_{VFT} and C_{VFT} is difficult. Nevertheless, C_{VFT} is often identified with the Kauzmann temperature (T_K) (Angell, 1997), at which the liquid and crystalline entropies are equal. At T_K, the VFT equation in combination with the Adam-Gibbs equation (Adam & Gibbs, 1965) yields a configurational entropy (S_c) of zero (Mauro et al., 2009; Scherer, 1992), although $S_c = 0$ is only possible at absolute zero temperature (Avramov & Milchev, 1988; Mauro et al., 2009). On the other hand, Gibbs and DiMarzio (1958) have derived a possible thermodynamic equilibrium glass transition. Overall the physical meaning of the VFT fitting parameters continue to be a subject of discussions (e.g., Hecksher et al., 2008; Schmelzer et al., 2018; Stillinger, 1988). Finally, the VFT equation is also known to break down at low T (Laughlin & Uhlmann, 1972; Mauro et al., 2009; Scherer, 1992).

Therefore, a physically based parametrization of η for glass-forming melts remains an interesting subject of research. For example, the viscosity description given in the model for glass-forming liquids by Adam and Gibbs (1965) (AG) has a physical foundation. It assumes the cooperative rearrangement of independent regions within the liquid and that the potential energy of the system can be expressed by its own partition function. This leads to

$$\log \eta = A_{\mathrm{AG}} + \frac{B_{\mathrm{AG}}}{TS_c}, \tag{4}$$

where $A_{\mathrm{AG}} = \log \eta_\infty$, and B_{AG} is an effective activation barrier (Adam & Gibbs, 1965; Richet, 1984). As the configurational entropy S_c cannot be measured, the use of the AG equation requires an additional fit for S_c at T_g and the measurement of configurational heat capacity of the melt ($C_{P,\mathrm{conf}}$) via DSC (Bouhifd et al., 2006;

Di Genova, Romano, Giordano, & Alletti, 2014; Giordano & Russell, 2017; Richet, 1987; Robert et al., 2014; Russell & Giordano, 2017; Sehlke & Whittington, 2016; Stebbins et al., 1984; Toplis, 1998; Webb, 2008).

One can avoid fitting S_c and measuring $C_{P,\mathrm{conf}}$ by using the MYEGA model by Mauro et al. (2009). It describes S_c in the AG expression (Equation 4) using constraint theory and an energy landscape analysis, and takes the form

$$\log\eta = A + \frac{K}{T}\exp\left(\frac{C}{T}\right), \tag{5}$$

where A, K and C are fitting parameters, with $A = \log\eta_\infty$ as above. An alternative, physically insightful, parametrization of Equation 5, suggested by Mauro et al. (2009), can be obtained by inserting the definition of T_g (Equation 1) and making use of the steepness index m (fragility), which quantifies the deviation of η from Arrhenian behavior at T_g (Angell, 1995),

$$m = \left(\frac{\partial\log\eta}{\partial(T_g\,/\,T)}\right)_{T=T_g} = \frac{K}{T_g}\left(1+\frac{C}{T_g}\right)\exp\left(\frac{C}{T_g}\right). \tag{6}$$

Reformulating Equation 5 with respect to these parameters yields:

$$\log\eta = A + (12-A)\frac{T_g}{T}\exp\left[\left(\frac{m}{12-A}-1\right)\left(\frac{T_g}{T}-1\right)\right]. \tag{7}$$

An analogous reformulation can be performed for the VFT model (Equation 3):

$$\log\eta = A_{\mathrm{VFT}} + \frac{(12-A_{\mathrm{VFT}})^2}{m_{\mathrm{VFT}}(T\,/\,T_{g,\mathrm{VFT}}-1)+(12-A_{\mathrm{VFT}})}. \tag{8}$$

A comparison between the performance of the MYEGA (Equation 7) and VFT models (Equation 8), using anhydrous simple and multicomponent oxide systems, that is, technical glasses, and molecular liquids covering a wide range of m from 20 to 115, revealed that the MYEGA equation provides a superior fit for η in all systems (Mauro et al., 2009). Moreover, using 568 different technical silicate liquids with widely varying compositions and η data in the range of 10^1–10^6 Pa s, Mauro et al. (2009) also showed that the MYEGA model predicted the 10^{11} Pa s isokom T better. Finally, unlike the VFT parametrization, the MYEGA equation offers a realistic extrapolation of S_c to both the high- and low-T limits, with consequences for the estimate of A and the description of the low-T scaling for η (Mauro et al., 2009).

2.2. Modeling the Effect of Water on the Viscosity of Silicate Melts

The presence of water in volcanic melts adds complexity to fitting η, as even a small amount of H_2O generally leads to a strong decreases of η. While the Hη and Lη regimes are usually accessible for anhydrous melts and provide strong constraints on the parametrization over a large η range, the lack of Lη data for hydrous compositions challenges the quality of the fit. This can lead, for example, to an unphysical crossover of η at different H_2O content when viscosity is extrapolated to the Lη domain (Figure S1). To avoid η crossovers, A_{VFT}, B_{VFT}, and C_{VFT} in Equation 3 are often empirically expressed as a function of H_2O content (e.g., Giordano et al., 2008, 2009; Hess & Dingwell, 1996; Romine & Whittington, 2015; Vetere et al., 2013; Whittington et al., 2009). While resulting fits usually provide a good description, there is no systematic approach and no physical interpretation of parameters involved, which results in a plethora of different models based on VFT.

Here we expand the MYEGA parametrization (Equation 7) in a physically motivated way to fit anhydrous and hydrous data for a given volcanic melt with varying H_2O content. We assume A to be independent of H_2O content (i.e., fixed by the anhydrous measurements), which reduces the water-dependent parameters to m and T_g. We base our η description on a T_g model by Schneider et al. (1997), who implemented a power concentration expansion of the Gordon-Taylor equation (Gordon & Taylor, 1952).

$$T_g(x_{H_2O}) = w_1T_{g,H_2O} + w_2T_{g,d} + cw_1w_2(T_{g,d}-T_{g,H_2O}) + dw_1w_2^2(T_{g,d}-T_{g,H_2O}), \tag{9}$$

with

$$w_1 = \frac{x_{H_2O}}{b(100 - x_{H_2O}) + x_{H_2O}} \quad \text{and} \quad w_2 = \frac{b(100 - x_{H_2O})}{b(100 - x_{H_2O}) + x_{H_2O}}, \tag{10}$$

where $T_{g,d}$ is the glass transition T of the anhydrous (dry) composition and T_{g,H_2O} that of water (136 K, −137 °C) (Kohl et al., 2005); x_{H_2O} is given in mol%. There are three fitting parameters in this H_2O-dependent model of T_g: b, c and d.

Reformulating the MYEGA equation (Equation 5), m can be expressed as

$$m = (12 - A)\left[1 + \ln\left(\frac{12 - A}{K} T_g\right)\right]. \tag{11}$$

Assuming that the parameter K does not depend on x_{H_2O}, that is, takes the value of the anhydrous melt results in m, depending on H_2O content through $T_g(x_{H_2O})$ only,

$$m = m_d + (12 - A)\ln\left(\frac{T_g}{T_{g,d}}\right). \tag{12}$$

The parameter m_d is the melt fragility of the anhydrous sample.

2.3. Fitting the Viscosity of Hydrous Silicate Melts

To fit a set of viscosity data including anhydrous and hydrous measurements of one specific melt composition, we follow these steps:

1. We fit the anhydrous data using the MYEGA model (Equation 7). These data sets often include Hη and Lη measurements constraining the values of A, $T_{g,d}$ and m_d well.
2. We insert Equations 9 and 12 into the MYEGA equation (Equation 7) and fit the resulting model to the remaining hydrous data. This constrains parameters b, c and d.

To evaluate the quality of the fit, we employ the root-mean-square error (RMSE),

$$RMSE = \sqrt{\frac{\sum_{n=1}^{N}(\eta_{c,n} - \eta_{m,n})^2}{N}}, \tag{13}$$

where $\eta_{c,n}$ and $\eta_{m,n}$ are calculated and measured values respectively. N is the number of data points for which the error is calculated.

3. Viscosity Database

We use 50 viscosity data sets (1,603 data points) from the literature for fitting (Tables 1–3), displayed in a TAS diagram (Figure 1). The data sets span a large compositional space with SiO_2 content ranging from 44 wt% to 79 wt% and total alkali content ranges from 0 wt% to 17 wt% (mol% reported in Tables 1–3). Virtually all types of magma erupted on Earth are represented.

Of the 50 data sets, 45 include viscosity measurements in the Hη and Lη region for anhydrous melts (Table 1), 26 sets additionally contain data for hydrous compositions (marked by * in Table 1 and listed in Table 2). All anhydrous data are used in Section 4 to explore the parameters A, m and T_g; in Section 5, we explore the quality of our model for the 26 H_2O-bearing liquids (Table 2).

Table 3 lists five data sets. One only includes anhydrous measurements, while for the remaining four anhydrous and hydrous measurements are available. The η values for melts in Table 3 are derived from DSC measurements using the approach reviewed in Stabile et al. (2021) (for further discussion see Section 6). They complement viscometry measurements on glasses from eruptions already included in our database (Tables 1 and 2). With DSC, η is determined in the Hη range only. In Section 6, we use DSC-derived η to illustrate that for high-quality data a reliable and predictive extrapolation of the MYEGA model from the H η to Lη range is possible, assuming a fixed value for A.

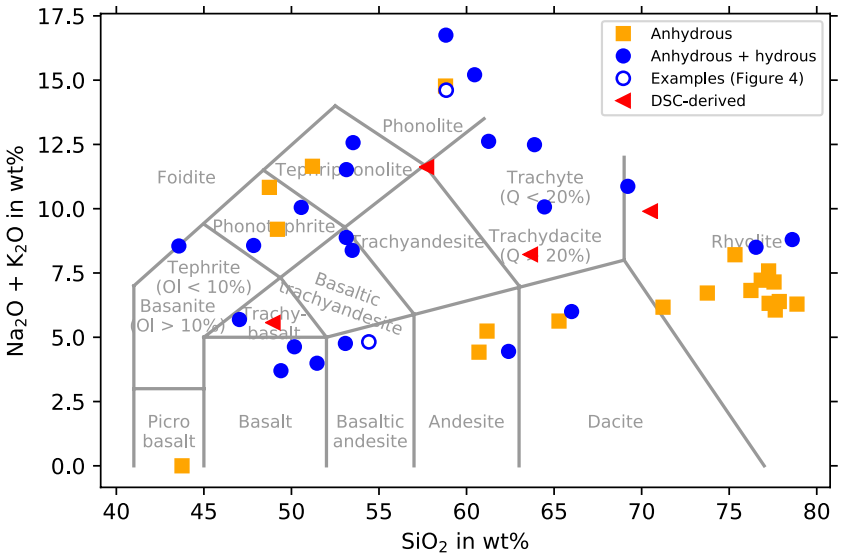

Figure 1. Total alkali-silica representation of the data sets used in our study (Tables 1–3). Data sets are color coded according to dry only data (orange squares), those including dry and hydrous data (blue) and differential scanning calorimetry (DSC)-derived viscosities (red triangles). Open blue circles denote samples that are used to illustrate the combined fits of the MYEGA (Equation 7) and H_2O model (Equations 9–12) in Section 5.

4. Anhydrous Melts

4.1. MYEGA Fit

We use the MYEGA (Equation 7) and VFT models (Equation 8) to fit η data from 45 different anhydrous silicate melts, all of which include measurements in the Hη and Lη range (MYEGA: Figure 2, VFT: Figure S3). Including Hη and Lη measurements provides a good constraint on the fits, as two of the parameters used in the MYEGA model, $T_{g,d}$ and m_d, are quantities defined at high η (Equations 1 and 6); A, on the other hand, is a low-η quantity for $T \rightarrow \infty$. Data and fits are grouped according to increasing SM values (Equation 2) in Figure 2. The often employed structural NBO/T parameter (Mysen, 1988) was not used as it correlates positively with the chemical parameter SM (Figure S2), and Giordano and Dingwell (2003a) have shown that SM is a valid empirical parameter to infer the degree of structural polymerization of the melt. Moreover, SM is easier to calculate and therefore used here.

Figure 2a shows measurements of samples with SM < 10, which are the most polymerized melts with $x_{SiO_2} > 80$ mol%. Their interval of η measurements ranges from 10^2 to 10^{13} Pa s, with 785 °C < T < 1650 °C. For these melts, the 1 / T dependence of η is quasi-linear, that is, they exhibit an Arrhenian behavior. Figure 2b displays η for liquids with 10 ≤ SM < 20. For these less polymerized melts, η and T ranges are $10^1 - 10^{14}$ Pa s, and 585 – 1710 °C, respectively. Some melts (e.g., Rhy14, Pho3) display Arrhenian behavior, while others (e.g., Rhy12, And3) exhibit a weak, but significant departure from linearity, that is, behave in a non-Arrhenian fashion. Figure 2c shows η data and fits for relatively depolymerized melts with 20 ≤ SM < 30. Viscosity measurements range from 10^{-1} to 10^{14} Pa s, and 615 – 1570 °C. The majority of these melts exhibit a pronounced non-Arrhenian behavior for η, with the exception of the shoshonite sample (Sho), for which the Lη range appears poorly constrained (see discussion on A below). Finally, Figure 2d shows η for the most depolymerized melts with SM ≥ 30, with 10^0 Pa s < η < 10^{14} Pa s and 635 °C < T < 1560 °C. Our results thus agree with the expected scenario that Arrhenian liquids are characterized by a polymerized melt structure due to their high content of network-forming cations (low SM), while liquids with larger values of SM exhibit non-Arrhenian behavior (e.g., Angell, 1995; Mysen, 1988; Ni et al., 2015).

Fitting parameters A, T_g and m are shown as a function of SM in Figure 3 for the MYEGA model. The fits reveal a steep decrease in T_g from 842 °C (Rhy2) to 741 °C (Rhy10) for the most polymerized melts in the interval 6.5 ≤ SM ≤ 10 (Figure 3b); with further increase of SM to 48.9 (Foi), T_g decreases to 643 °C. This behavior reflects the control of melt structure on T_g: Highly polymerized melts exhibit high T_g, and the addition of a

Geochemistry, Geophysics, Geosystems

10.1029/2021GC009918

Table 1

Viscosity Data Sets for Anhydrous Volcanic Melts Used for Fitting, Ordered With Increasing SM *Values*

Sample	# data	SM	SiO_2	TA	$A_{MYEGA,free}$	$T_{g,MYEGA,free}$ in K	$m_{MYEGA,free}$	RMSE	$A_{MYEGA,fixed}$	$T_{g,MYEGA,fixed}$ in K	$m_{MYEGA,fixed}$	RMSE	Reference	Comment
Rhy1	12	6.49	85.04	4.69	−7.76	1095.64	20.53	0.0005	−2.90	1105.36	25.15	0.0065	Di Genova, Kolzenburg, et al. (2017)	F
Rhy2	13	7.29	84.40	4.80	−5.56	1115.22	24.47	0.0022	−2.90	1121.23	27.57	0.0053	Di Genova, Kolzenburg, et al. (2017)	G
Rhy3	16	7.60	83.06	5.30	−9.60	1074.05	20.40	0.0057	−2.90	1093.07	27.11	0.0240	Di Genova, Kolzenburg, et al. (2017)	B
HPG8*	10	7.66	84.36	7.66	−7.24	1104.47	21.86	0.0012	−2.90	1116.93	26.57	0.0076	Hess et al. (1995); Dingwell et al. (1996)	HPG8
Rhy4	11	7.86	83.72	6.02	−6.82	1071.05	20.93	0.0002	−2.90	1083.97	25.25	0.0046	Di Genova, Kolzenburg, et al. (2017)	C
Rhy5	12	8.23	82.92	5.70	−4.07	1041.24	23.75	0.0008	−2.90	1043.84	25.31	0.0014	Di Genova, Kolzenburg, et al. (2017)	A
Rhy6	14	8.53	82.73	6.01	−5.85	1090.66	23.81	0.0057	−2.90	1097.45	27.28	0.0096	Di Genova, Kolzenburg, et al. (2017)	D
Rhy7	13	8.68	81.75	6.19	−6.29	1098.80	23.06	0.0033	−2.90	1108.12	26.91	0.0072	Di Genova, Kolzenburg, et al. (2017)	E
Rhy8*	20	8.87	82.57	7.21	−5.76	1080.59	22.63	0.0037	−2.90	1086.70	25.38	0.0113	Romine and Whittington (2015)	NCA
Rhy9	13	9.13	82.58	6.31	−4.75	1056.17	23.67	0.0013	−2.90	1064.76	26.28	0.0023	Di Genova, Kolzenburg, et al. (2017)	H
Rhy10	12	9.33	82.57	5.78	−5.19	1014.28	21.95	0.0003	−2.90	1022.08	24.97	0.0021	Di Genova, Kolzenburg, et al. (2017)	I
Rhy11	15	13.18	78.27	5.66	−3.35	990.27	26.17	0.0005	−2.90	992.25	26.99	0.0007	Di Genova, Kolzenburg, et al. (2017)	J
Rhy12	12	13.92	77.38	5.32	−3.58	1095.56	34.27	0.0092	−2.90	1097.87	35.77	0.0097	Di Genova, Kolzenburg, et al. (2017)	L
Tra1*	18	15.25	72.30	11.14	−5.51	924.83	22.50	0.0005	−2.90	936.96	26.28	0.0069	Giordano et al. (2004)	MNV
Rhy14*	12	15.25	72.30	11.14	−2.69	814.70	23.92	0.0028	−2.90	813.46	23.54	0.0028	Di Genova et al. (2013)	PS-GM
Tra2*	18	15.49	70.26	10.58	−3.78	1020.82	30.65	0.0057	−2.90	1023.87	32.22	0.0067	Giordano et al. (2004)	IGC
Dac1	12	16.08	71.31	5.49	−4.49	957.68	27.46	0.0015	−2.90	965.04	30.67	0.0045	Alidibirov et al. (1997)	
Dac2*	20	16.95	71.91	5.56	−2.71	982.09	32.91	0.0016	−2.90	981.11	32.49	0.0017	Giordano and Dingwell (2003a)	UNZ
Pho1*	22	17.23	67.99	13.83	−5.16	920.36	23.37	0.0014	−2.90	929.29	26.90	0.0113	Giordano et al. (2009)	Mercato1600 with hydrous data
Pho2	13	17.29	67.97	13.98	−4.88	911.56	23.42	0.0001	−2.90	919.36	26.25	0.0022	Giordano et al. (2009)	Mercato1400
Dac3*	50	17.40	69.43	6.07	−3.36	1034.29	34.96	0.0010	−2.90	1035.17	35.87	0.0018	Whittington et al. (2009)	BRD
Tra3*	11	17.42	69.13	10.80	−3.42	933.24	25.16	0.0067	−2.90	935.28	25.96	0.0070	Romano et al. (2003)	AMS_B1

Geochemistry, Geophysics, Geosystems

10.1029/2021GC009918

Table 1
Continued

Sample	# data	SM	SiO_2	TA	$A_{MYEGA,free}$	$T_{g,MYEGA,free}$ in K	$m_{MYEGA,free}$	RMSE	$A_{MYEGA,fixed}$	$T_{g,MYEGA,fixed}$ in K	$m_{MYEGA,fixed}$	RMSE	Reference	Comment
Pho3*	22	17.79	68.32	14.62	−4.53	874.37	22.71	0.0007	−2.90	879.95	25.14	0.0054	Giordano et al. (2000)	
And1	14	19.84	67.00	5.06	−2.67	958.51	33.61	0.0022	−2.90	958.20	33.02	0.0024	Neuville et al. (1993)	Andesite
And2*	36	19.90	66.89	4.29	−3.07	1016.50	35.79	0.0004	−2.90	1016.83	36.23	0.0006	Richet et al. (1996)	Andesite
And3	21	19.96	66.27	4.37	−3.38	951.40	32.77	0.0004	−2.90	953.00	33.98	0.0012	Giordano et al. (2006)	MST
Tra5*	24	20.05	68.95	9.25	−2.49	970.99	32.07	0.0014	−2.90	969.84	31.17	0.0023	Whittington et al. (2001)	Trachyte
Pho4*	20	21.20	65.35	15.30	−2.10	919.10	30.05	0.0011	−2.90	917.74	28.49	0.0049	Whittington et al. (2001)	Phonolite
Lat*	30	22.25	62.69	7.89	−3.56	968.03	34.64	0.0345	−2.90	969.76	36.28	0.0361	Misiti et al. (2011)	FR
Pho5*	14	24.41	60.62	10.83	−6.41	914.74	26.18	0.0061	−2.90	927.36	31.53	0.0202	Romano et al. (2003)	V_1631_W
BasAnd1*	22	24.45	59.42	4.86	−2.53	947.54	38.23	0.0017	−2.90	946.84	37.06	0.0023	Robert (2014)	fu18
Pho6*	14	24.79	60.26	11.23	−4.74	928.70	34.77	0.0238	−2.90	943.04	31.20	0.0356	Romano et al. (2003)	V_1631_G
TepPho1	12	26.29	58.81	9.96	−4.08	939.20	32.87	0.0018	−2.90	944.01	36.22	0.0032	Giordano and Dingwell (2003a)	Ves_W_tot
Sho*	10	29.22	58.74	7.21	−9.44	903.15	25.47	0.0027	−2.90	911.67	35.39	0.0674	Vetere et al. (2007)	Vul
BasAnd2*	24	29.27	56.94	4.52	−3.13	988.47	40.22	0.0019	−2.90	988.73	40.93	0.0022	Robert et al. (2013)	sba
TepPho2	14	30.23	55.33	9.15	−2.72	942.93	40.31	0.0020	−2.90	942.45	39.77	0.0021	Giordano et al. (2009)	Pollena GM
Bas1*	10	30.50	53.60	5.55	−3.17	958.76	43.46	0.0016	−2.90	959.68	44.75	0.0017	Giordano and Dingwell (2003b)	ETN
Bas3*	25	31.24	54.08	3.71	−2.25	932.19	44.40	0.0019	−2.90	931.16	41.67	0.0051	Robert et al. (2015)	fu06
Bas4*	26	31.54	54.33	4.12	−3.00	932.17	40.63	0.0054	−2.90	932.74	41.02	0.0054	Misiti et al. (2009); Giordano et al. (2006)	SPZ, STB
TepPho3	16	31.65	54.80	7.53	−3.61	942.62	37.68	0.0022	−2.90	945.94	40.24	0.0034	Giordano and Dingwell (2003a)	Ves_G_tot
PhoTep1*	14	32.49	53.59	7.00	−2.51	937.95	42.26	0.0008	−2.90	937.30	40.97	0.0013	Giordano et al. (2009)	1906GM
Bas5*	33	36.10	51.89	3.66	−3.26	982.93	43.47	0.0024	−2.90	983.34	44.88	0.0031	Robert et al. (2015)	sb
Tep*	22	38.47	51.29	8.87	−1.85	932.49	48.96	0.0011	−2.90	930.00	44.48	0.0102	Whittington et al. (2000)	Tephrite
Foi*	20	48.87	42.95	7.86	−2.80	915.88	49.77	0.0009	−2.90	915.84	49.57	0.0010	Whittington et al. (2000)	NIQ
Di	37	56.19	43.75	0.00	−2.16	997.87	61.12	0.0013	−2.90	996.22	55.70	0.0066	Al-Mukadam et al. (2020)	Di

Note. The first block lists chemical composition (total alkaline TA and SiO_2 given in mol%) and contains information on the data. The second block provides fitting parameters for the MYEGA equation (Equation 7), the third block the MYEGA fit with constant $A = -2.9$, both listing the RMSE (Equation 13) of the fits. The final block contains the references from which data are taken and the column "Comment" refers to the sample name in the respective reference. The symbol * denotes samples for which hydrous compositions are also available (Table 2). And, Andesite; Bas, Basalt; BasAnd, Basaltic Andesite; Dac, Dacite; Di, Diopside; Foi, Foidite; HPG-Haplogranite; Lat, Latite; Pho, Phonolite; PhoTep, Phonotephrite; Rhy, Rhyolite; RMSE, root-mean-square error; Sho, Shoshonite; Tep, Tepherite; TepPho, Tephriphonolite; Tra, Trachyte.

Geochemistry, Geophysics, Geosystems

10.1029/2021GC009918

Table 2

Viscosity Data Sets From Viscometry Measurements for Hydrous Melts Used for Fitting, Ordered With Increasing SM *Value*

Sample	# dry data	SM	SiO_2	TA	H_2O range	# hydrous data	A	$T_{g,d}$	m_d	b	c	d	RMSE	$RMSE_{lit}$	$RMSE_{GRD}$	$RMSE_{HZ}$	$RMSE_{Duan}$	Reference	Comment
HPG8	10	7.66	84.36	7.66	0–11.04	22	−7.24	1104.47	21.86	0.09	1.18	−1.90	0.17		0.83	0.36		Hess et al. (1995); Dingwell et al. (1996)	HPG8
Rhy8	20	8.87	82.57	7.21	0–1.21	130	−5.76	1080.59	22.63	8.26	60548.14	−60715.84	0.09		0.73	0.35	3.64	Romine and Whittington (2015)	NCA
Tra1	18	15.25	72.30	11.14	0–13.06	13	−5.51	924.83	22.50	0.24	1.07	−1.66	0.08	0.11	0.14	0.20	1.35	Giordano et al. (2004)	MNV
Rhy14	12	15.25	72.30	11.14	0–11.91	15	−2.69	814.70	23.92	0.16	1.51	−2.08	0.17	0.13	1.38	0.50	2.98	Di Genova et al. (2013)	PS-GM
Tra2	18	15.49	70.26	10.58	0–11.77	17	−3.78	1020.82	30.65	0.07	1.89	−2.26	0.10	0.10	0.42	0.34	0.87	Giordano et al. (2004)	IGC
Dac2	20	16.95	71.91	5.56	0–6.80	9	−2.71	982.09	32.91	45.08	49658.91	−49909.83	0.17	0.17	0.39	0.28	0.10	Giordano and Dingwell,(2003a)	UNZ
Pho1	22	17.23	67.99	13.83	0–14.46	30	−5.16	920.36	23.37	0.08	1.85	−1.83	0.22	0.22	0.34	0.35	1.17	Giordano et al. (2009)	Mercato 1600 with hyd. data
Dac3	50	17.40	69.43	6.07	0–16.06	26	−3.36	1034.29	34.96	0.14	1.52	−2.02	0.15	0.20	0.53	0.38		Whittington et al. (2009)	BRD
Tra3	11	17.42	69.13	10.80	0–12.91	23	−3.42	933.24	25.16	9.51	1926.67	−1979.48	0.12	0.21	0.37	0.22	1.14	Romano et al. (2003)	AMS_B1
Pho3	22	17.79	68.32	14.62	0–12.79	15	−4.53	874.37	22.71	0.13	1.68	−2.05	0.11	0.10	0.42	0.30	1.17	Giordano et al. (2000)	
And2	36	19.90	66.89	4.29	0–11.35	45	−3.07	1016.50	35.79	0.29	1.73	−2.57	0.10		0.34	0.24	1.59	Richet et al. (1996)	
Tra5	24	20.05	68.95	9.25	0–15.60	42	−2.49	970.99	32.07	0.20	1.01	−1.44	0.17		0.44	0.39		Whittington et al. (2001)	Trach
Pho4	20	21.20	65.35	15.30	0–14.19	36	−2.10	919.10	30.05	4.68	278.56	−300.15	0.35		0.67	0.66		Whittington et al. (2001)	Phon
Lat	30	22.25	62.69	7.89	0–11.31	21	−3.56	968.03	34.64	0.04	3.03	−3.13	0.19	0.22	0.47	0.53	0.93	Misiti et al. (2011)	FR
Pho5	14	24.41	60.62	10.83	0–11.52	14	−6.41	914.74	26.18	1.06	21.86	−27.14	0.09	0.21	0.74	0.25	0.79	Romano et al. (2003)	V_1631_W
BasAnd1	22	24.45	59.42	4.86	0–10.03	23	−2.53	947.54	38.23	0.45	1.66	−2.69	0.07	0.09	0.51	0.31	1.07	Robert (2014)	fu18
Pho6	14	24.79	60.26	11.23	0–10.71	11	−5.67	935.17	27.17	0.97	19.58	−24.68	0.13	0.23	0.69	0.34	0.92	Romano et al. (2003)	V_1631_G
Sho	10	29.22	58.74	7.21	0–15.43	15	−9.44	903.15	25.47	0.41	0.74	−1.17	0.11	0.16	0.46	0.98	1.04	Vetere et al. (2007)	Vul
BasAnd2	24	29.27	56.94	4.52	0–12	32	−3.13	988.47	40.22	0.09	1.98	−1.85	0.13	0.24	0.72	0.50		Robert et al. (2013)	sba

Geochemistry, Geophysics, Geosystems

10.1029/2021GC009918

Table 2
Continued

Sample	# dry data	SM	SiO_2	TA	H_2O range	# hydrous data	A	$T_{g,d}$	m_d	b	c	d	RMSE	$RMSE_{lit}$	$RMSE_{GRD}$	$RMSE_{HZ}$	$RMSE_{Duan}$	Reference	Comment
Bas1	10	30.50	53.60	5.55	0–8.1	18	−3.17	958.76	43.46	0.10	2.00	−2.01	0.18	0.23	0.42	0.36	1.05	Giordano and Dingwell (2003b); Giordano et al. (2009)	ETN
Bas3	25	31.24	54.08	3.71	0–9.12	25	−2.25	932.19	44.40	0.62	0.00	−0.91	0.09	0.11	0.76	0.64	1.16	Robert et al. (2015); Robert (2014)	fu06
Bas4	26	31.54	54.33	4.12	0–13.58	17	−3.00	932.17	40.63	0.14	1.64	−1.54	0.19	0.21	0.56	0.47	0.78	Misiti et al. (2009); Giordano et al. (2006, 2009)	SPZ, STB, STR
PhoTep1	14	32.49	53.59	7.00	0–14.71	16	−2.51	937.95	42.26	0.11	2.02	−2.05	0.24	0.51	0.62	0.80	1.10	Giordano et al. (2009)	1906GM
Bas5	33	36.10	51.89	3.66	0–9.44	26	−3.26	982.93	43.47	0.10	1.64	−1.22	0.30	0.28	1.85	2.50		Robert et al. (2015); Robert (2014)	sb
Tep	22	38.47	51.29	8.87	0–7.34	31	−1.85	932.49	48.96	0.24	2.21	−2.39	0.20		1.14	0.51		Whittington et al. (2000)	Teph
Foi	20	48.87	42.95	7.86	0–5.96	32	−2.80	915.88	49.77	0.11	1.29	−0.81	0.10		0.69	0.24		Whittington et al. (2000)	NIQ

Note. The first block lists chemical composition (including the H_2O content in mol%) and contains information on the data, the third block information on references. In the second block the fitting parameters for the hydrous MYEGA model (Equations 7, 9 and 10) and the RMSE are given, with the RMSE compared to the literature fits as well as general chemical models: GRD for Giordano et al. (2008), HZ for Hui and Zhang (2007), Duan for Duan (2014). "Comment" refers to the sample name in the respective reference. Measurements mentioned to have crystallized/lost water and so on in the respective reference are excluded from fitting. And, Andesite; Bas, Basalt; BasAnd, Basaltic Andesite; Dac, Dacite; HPG-Haplogranite; Lat, Latite; Pho, Phonolite; PhoTep, Phonotephrite; Rhy, Rhyolite; RMSE, root-mean-square error; Sho, Shoshonite; Tep, Tepherite; Tra, Trachyte.

Table 3
Differential Scanning Calorimetry (DSC)-Derived Viscosity Data Sets Used for Fitting, Ordered With Increasing SM

Sample	# dry data	SM	SiO_2	TA	H_2O range	# hydrous data	A	$T_{g,d}$	m_d	b	c	d	RMSE	Reference	Comment
Rhy14-DSC	4	14.16	77.46	9.06	0–11.91	16	−2.93	799.49	20.23	0.09	1.82	−1.99	0.14	Di Genova, Romano, Giordano, and Alletti (2014)	PS
Tra3-DSC	4	19.85	66.14	9.91	0–15.96	16	−2.93	910.88	25.11	0.24	0.95	−1.27	0.17	Di Genova, Romano, Giordano, and Alletti (2014)	AMS-B1
Lat-DSC	4	22.06	63.56	8.20	0–5.71	4	−2.93	929.95	33.36	0.98	1.53	−4.64	0.25	Di Genova, Romano, Giordano, and Alletti (2014)	FR
Bas1-DSC	4	31.19	53.82	5.26	0–8.30	8	−2.93	909.08	40.35	1.12	1.75	−4.61	0.53	Di Genova, Romano, Giordano, and Alletti (2014)	ETN
Di-DSC	10	56.19	43.75	0.00			−2.93	1000.06	59.14				0.09	Al-Mukadam et al. (2020)	Di

Note. The first block lists chemical composition (including the H_2O content in mol%) and contains information on the data, the third block information on references. In the second block the fitting parameters for the constrained hydrous MYEGA model (Equation 7 with $A = -2.9$, 9, and 10) and the RMSE are given. "Comment" indicates the sample name in the respective publication. Measurements mentioned to have crystallized/lost water and so on in the respective reference are excluded from fitting. Bas, Basalt; Di, Diopside; Lat, Latite; Rhy, Rhyolite; RMSE, root-mean-square error; Tra, Trachyte.

small amount of network modifying cations leads to a dramatic decrease in T_g. Rhy14 with SM = 14.6 shows T_g significantly lower than its low-SM SiO_2-rich counterparts. Rhy14 is a peralkaline rhyolite (pantellerite), characterized by an excess of alkali and alkaline earth cations over Al_2O_3 which induces a dramatic depolymerization of the melt structure within rhyolite chemistry (Di Genova et al., 2013; Dingwell et al., 1998a), leading to relatively low η (Figure 2b). As expected from Figure 2, melt fragility (m) positively correlates with SM (Figure 3c). In particular, we find that the strongest melt (m = 20.4) is Rhy3 with SM = 7.6, the most fragile melt is Di (m = 61.1) with SM = 56.2 (Table 1).

Finally, the parameter A increases significantly from −9.6 for Rhy3 to −1.9 for Tep with SM (Figure 3a, Table 1). We find the largest variation of A for SM < 10, and a relatively constant value of $A \sim -3$ for SM > 20. The low values of A for the polymerized melts with SM < 10 is likely caused by the limited η range accessible for measurements in the laboratory. For example, the viscosity of the polymerized melt Rhy3 (SM = 7.6, A = –9.6) that follows an Arrhenian behavior (Figure 2a), was measured in the range of $3.24 < \log\eta < 11.15$ (T < 1591 °C. It is not possible to extend measurements to significantly lower η values for such polymerized melts with T becoming too high for the measuring system and causing volatilization of alkalis from the melt. Therefore, A is not well constrained by this measurement interval. The sample Sho deviates from the expected behavior with SM = 29.3 and A = –9.4. This is a very low value of A compared to melts with similar SM. For Sho, only three data points exist in the Lη range with the lowest measured viscosity $\log\eta = 1.27$ (Vetere et al., 2007). This restricted Lη range may not permit an accurate determination of the T dependence in the Lη region and thus a reliable estimate of A.

4.2. The Viscosity at Infinite Temperature

A common assumption is that the viscosity of glass-forming melts converge to constant value of A as $T \to \infty$ (Angell et al., 2000), an assumption that can be integrated into the fitting by fixing the parameter A (Section 2.1). Maxwell's equation $\eta = G_\infty \tau$ provides an order-of-magnitude estimate. G_∞ is the shear modulus at infinite frequency and τ the relaxation time. For silicate melts at infinite T, they are estimated as $G_\infty = 10^{10}$ Pa (Dingwell & Webb, 1989) and $\tau_\infty \approx 10^{-14}$ s (Angell, 1997; Börjesson et al., 1987; Fujimori & Oguni, 1995), resulting in $A = \log\eta_\infty = -4$.

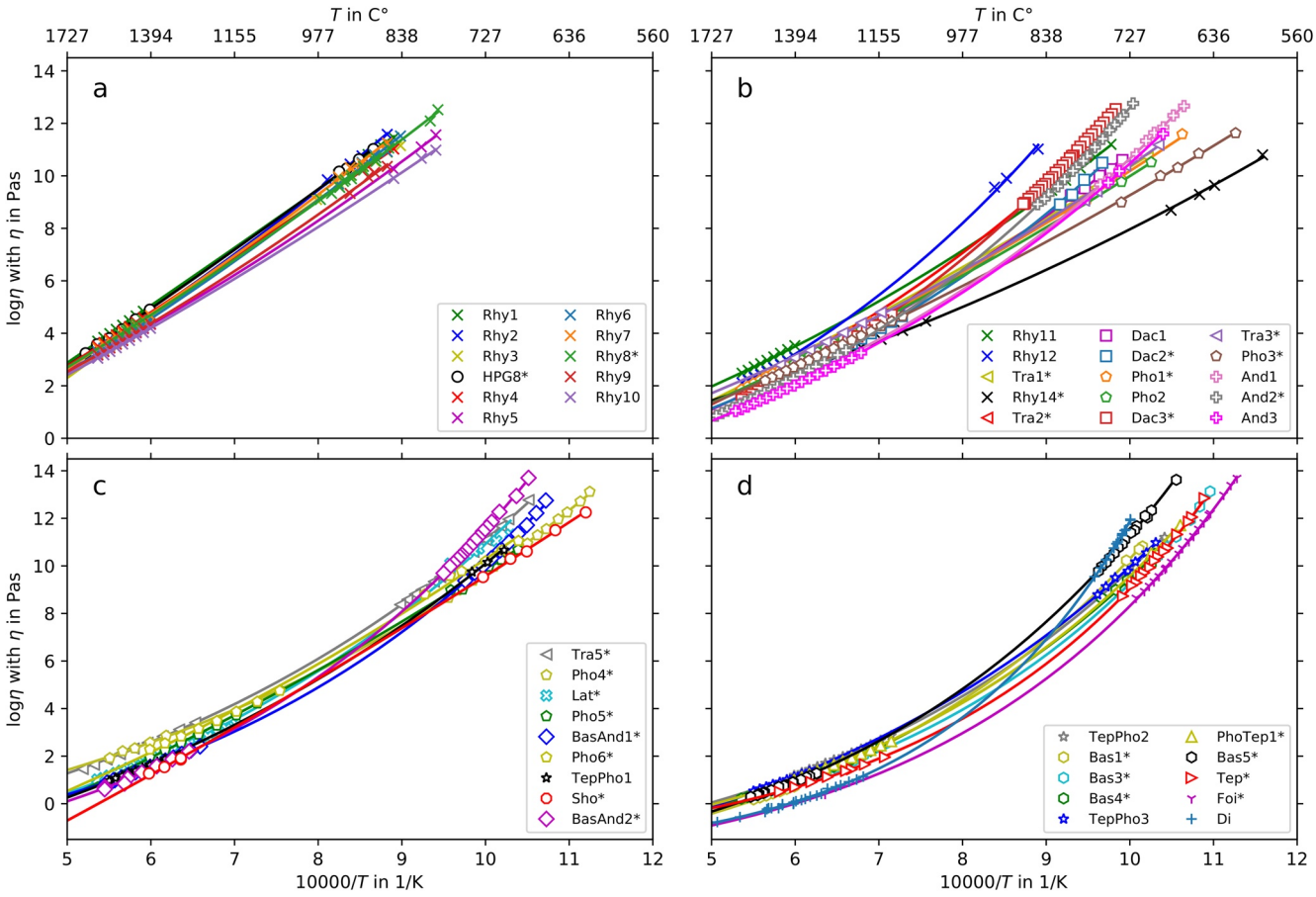

Figure 2. Fits to viscosity measurements of 45 anhydrous samples (Table 1) using the MYEGA model (Equation 7). Data are grouped according to the chemical parameter SM (Equation 2): Intervals are (a) SM < 10, (b) 10 ≤ SM < 20, (c) 20 ≤ SM < 30 and (d) SM ≥ 30. A corresponding figure using the VFT model (Equation 8) can be found in the Supporting Information (Figure S3). Abbreviations and references for the different data sets can be found in Table 1: * denotes samples for which hydrous measurements are also reported (Table 2). Symbols are assigned as follows: X for rhyolites, empty circles for HPG8, triangles to the left for trachytes, squares for dacites, pentagons for phonolites, empty crosses for andesites, empty X for latites, diamonds for basaltic andesites, stars for tephri-phonolites, octagons for shoshonite, hexagons for basalts, upwards triangles for phono-tephrites, triangles to the right for tephrites, tripods for foidite, crosses for diopside.

The VFT (Equation 3) and AG models (Equation 4) have been used in the literature to explore the range of A values for volcanic melts. Russell et al. (2003) obtained an average $\overline{A} = -4.3 \pm 0.7$ (VFT) and $\overline{A} = -3.2 \pm 0.7$ (AG) for a compilation of 20 silicate melts. Subsequent work by Giordano et al. (2008) included more data (198 compositions) and found a value of $\overline{A} = -4.6 \pm 0.2$ using a VFT equation dependent on chemical composition. For 946 technical silicate and 31 other glass-forming technical liquids, Zheng et al. (2011) determined $\overline{A} = -2.9 \pm 0.3$ for MYEGA (Equation 7) and $\overline{A} = -3.9 \pm 0.3$ for VFT. The literature data as well as the discussion by Mauro et al. (2009) show that the MYEGA model results in a larger value for $\overline{A}$ than VFT.

We observe a larger $\overline{A}$ for MYEGA than VFT with $\overline{A}_{\mathrm{MYEGA}} = -4.3 \pm 1.9$ and $\overline{A}_{\mathrm{VFT}} = -5.1 \pm 1.5$, respectively. The difference between them is consistent with the results of Zheng et al. (2011). The trend to low values of A that we observe stems largely from the 11 Arrhenian data sets with SM < 10 for which the quasi-linear extrapolation of η to high T yields very low values of A (Figure 3). When the eleven A values for melts with SM < 10 are excluded from averaging, $\overline{A}_{\mathrm{VFT}} = -4.6 \pm 1.2$, in agreement with the value found by Giordano et al. (2008) and close to that of Russell et al. (2003). Nine of the 11 melts in Table 1 with SM < 10 were not used in these two studies, but we assume they would have a similar influence on the values of A. A significant—but smaller—difference in $\overline{A}$ remains compared to the technical data set of Zheng et al. (2011). Excluding the A values for SM < 10 for the MYEGA fits, we obtain $\overline{A}_{\mathrm{MYEGA}} = -3.7 \pm 1.5$.

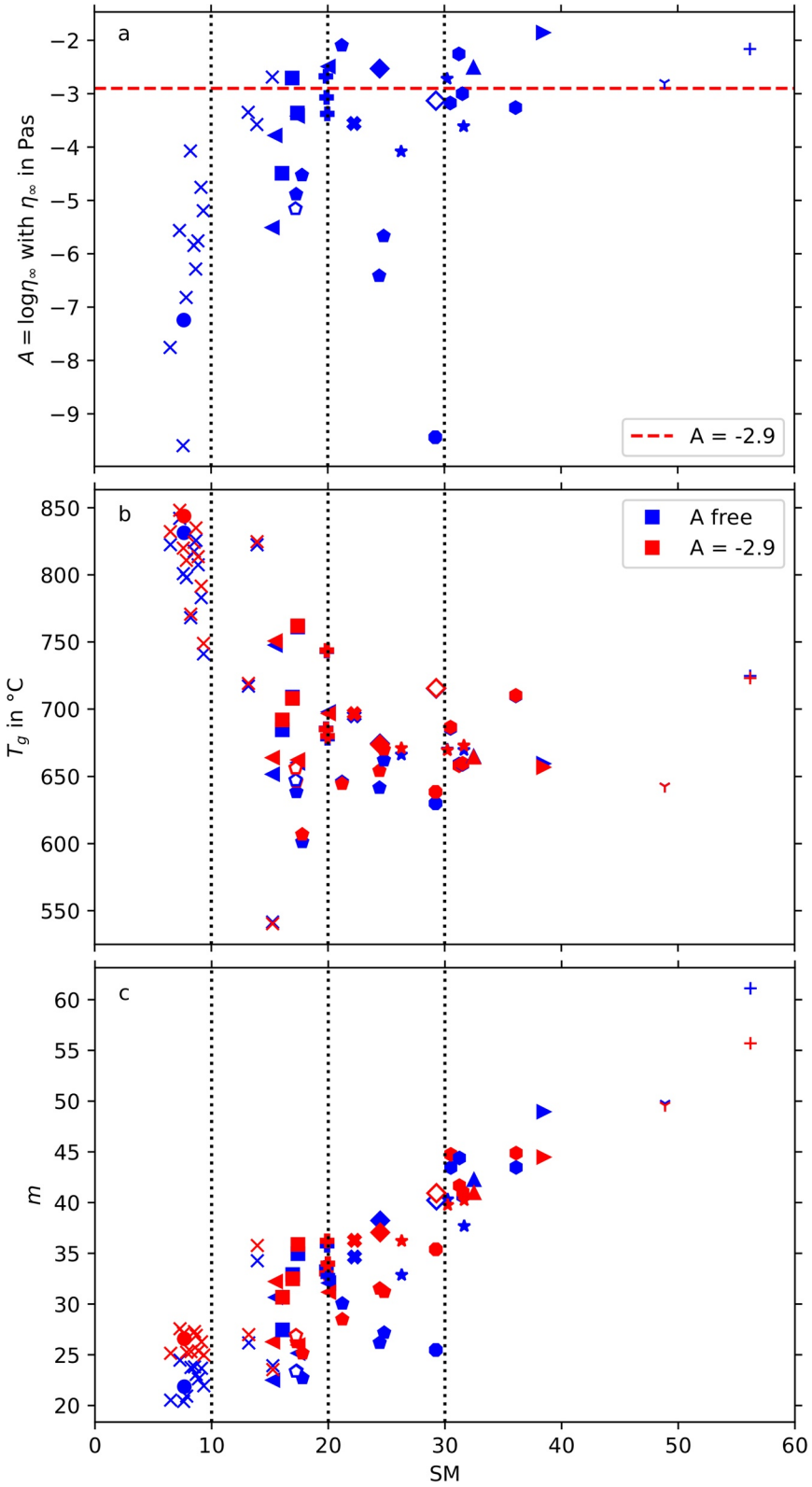

Figure 3. Values of the fitting parameters A (a), T_g (b), and m (c) calculated by applying the MYEGA model (Equation 7) to 45 anhydrous measurements, plotted against the structure parameter SM (Equation 2). Blue symbols are samples which were fit with parameter A free for optimization and red symbols used $A = -2.9$. Open symbols denote the two samples used as examples of hydrous melts in Section 5. Numerical values of fitting parameters for the MYEGA model can be found in Table 1. Symbols for different melt compositions are assigned according to Figure 2.

Low values of A also correlate with low values of the steepness factor (Figure 3), highlighting a difference between the current data set and that of Zheng et al. (2011). In their database, all $m > 25.9$. If we restrict averaging of A to melts with such m values, we obtain $\bar{A}_{\mathrm{MYEGA}} = -3.2 \pm 1.0$, in excellent agreement with Zheng et al. (2011). This underlines the observation that the measurable T interval for highly polymerized melts (low SM/low m) often is to narrow to constrain A.

4.3. Fitting With a Constant Value of A

In order to explore differences in the MYEGA fitting parameters when A is fixed or left as a free parameter, we refit the anhydrous data sets (Table 1) using $A = -2.9$ (Zheng et al., 2011). This may also be important for cases where only a small number of measurements over a limited Hη range are available, including DSC measurements which we address in Section 6. The RMSE values reported in Table 1 show an expected increase due to the reduction in fitting parameters, but overall the fitting quality is still high.

Values for T_g (Table 1 and Figure 3b) are very similar to the fits with free A since T_g is generally well constrained by measurements in the vicinity of $\eta = 10^{12}$ Pa s (Equation 1). The largest differences in T_g exist for melts with SM < 10, which exhibit the lowest values of A in the MYEGA fit and show quasi-Arrhenian behavior; with the shift of A to larger values, T_g are also shifted to larger values, but differences do not exceed 20 °C. For SM > 10, notable differences exist for Tra1 and Pho6. For these samples the lowest T of measurements is significantly larger than T_g (Figure 2), leading to a less effective constraint.

Similarly, m values for fixed $A = -2.9$ in the interval SM < 10 are systematically larger. This is readily rationalized by reversing the argument given in Section 4.2 that an Arrhenian behavior of η leads to small A. With $A = -2.9$ constrained, the fit is forced to become more non-Arrhenian, increasing the curvature near T_g. For $10 \leq \mathrm{SM} < 20$, the majority of m values associated with fixed A are larger but the deviation is less pronounced. In the interval SM ≥ 20, deviations are generally small and not systematic. A notable difference is Sho, for which Lη data are scarce as discussed in Section 4.1, with $m = 35.39$ for $A = -2.9$, compared to $m = 25.47$ for a fitted $A = -9.44$.

General trends discussed for the MYEGA fit with variable A are preserved for fixed $A = -2.9$, and become more systematic: T_g decreases with SM, and the fragility m increases with SM. Fixing A leads to a narrower distribution of m and indicates a quasi-linear correlation with SM.

5. Hydrous Silicate Melts

After fitting anhydrous viscosity data using the MYEGA model (Figure 2), we explore the H_2O-dependent model of Equations 9–12 for the 26 samples with hydrous data (Table 2). As examples, we show two compositions in Figure 4 that are also highlighted in Figures 1 and 3: a Basaltic Andesite (BasAnd2) (Robert et al., 2013) and a Phonolite (Pho1) (Giordano et al., 2009). The maximum H_2O content of the samples exceeds 11 mol% for viscosity measurements in the Hη range, with a large number of H_2O concentrations per composition (Table 2, Figure 4). The BasAnd2 data also include two falling sphere measurements of an H_2O bearing melts with 6.96 mol%. For both samples, H_2O-dependent models for η are published in the original work which provide a basis for comparing the quality of fits.

Our model describes the η measurements for BasAnd2 by Robert et al. (2013) significantly better than the literature model (Figure 4a)—with the exception of the two Lη falling sphere data—which is most clearly visible for 12 mol% H_2O. In addition, our model shows a tendency toward larger curvature in $\log\eta$ - $1/T$ (stronger non-Arrhenian behavior, larger m). For Pho1 (Figure 4d), the data are well described by both our fit and the model used in Giordano et al. (2009), with the exception of the highest H_2O content (14.39 mol%), which neither of the models match. With a high alkaline content (Figure 1 and Table 2), Pho1 shows Arrhenian behavior.

Through its definition (Equation 1), T_g is well constrained in all data sets by measurements in the Hη regime. Reported values and our results for BasAnd2 and Pho1 agree well, and T_g decreases monotonically with H_2O content. In our model, the extrapolation of T_g to 100 mol% H_2O is constrained to $T_{g,H_2O} = -137$° C (Kohl et al., 2005).

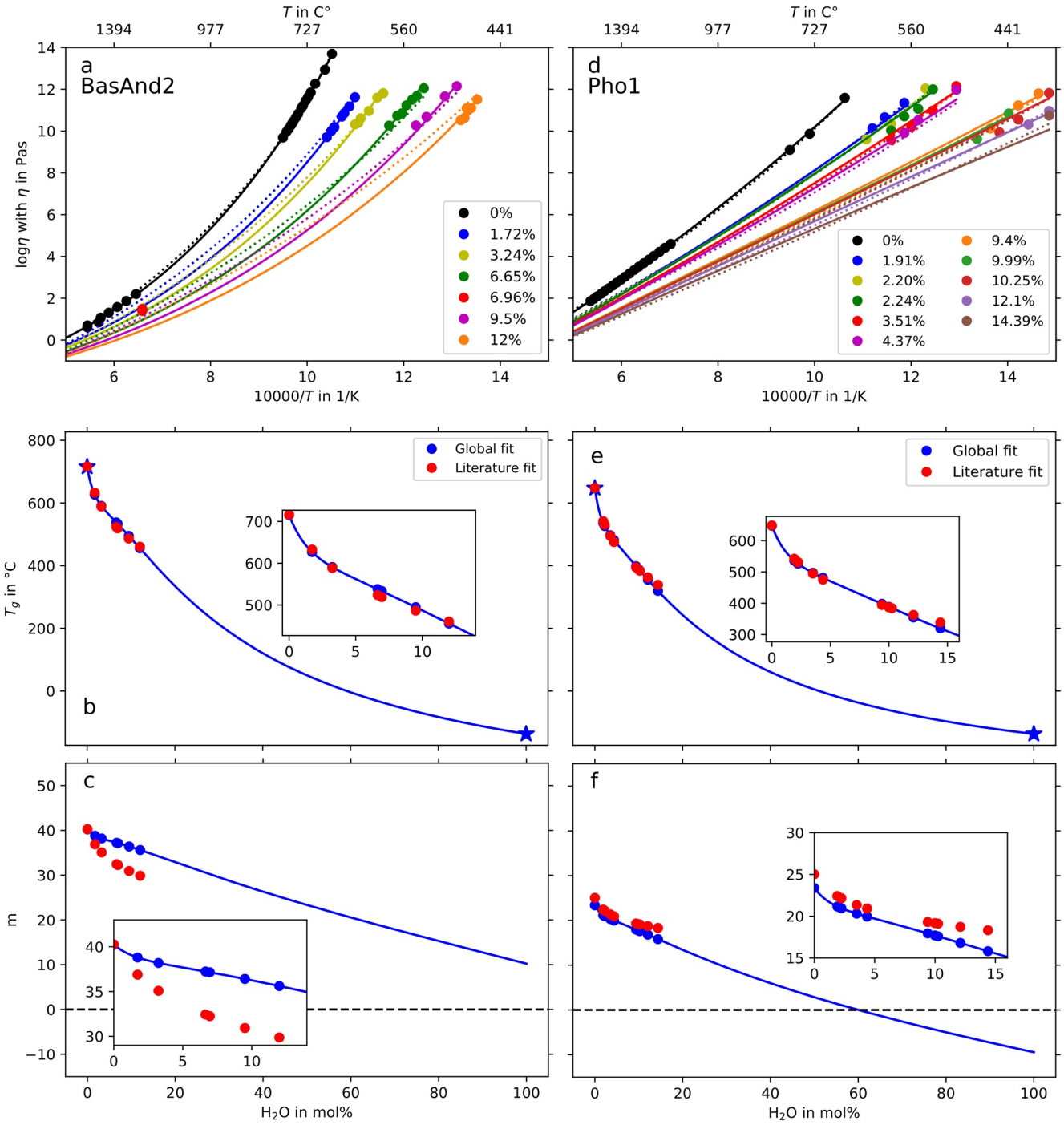

Figure 4. Hydrous viscosity data and fits for a Basaltic Andesite, BasAnd2 by Robert et al. (2013) (left column) and a Phonolite, Pho1 by Giordano et al. (2009) (right column). Solid lines are fits using the MYEGA model and the parametrization of water dependence formulated in the current work. Dotted lines show the fits for BasAnd2 and Pho1 from the original publications. Fitting parameters T_g (b and e) and m (c and f) for BasAnd2 and Pho1 were calculated by applying our parametrization (blue) and using the model given in the respective reference (red) to each data set of constant H_2O content. The insets cover the H_2O -content of the experiments, the full figures show the extrapolation to 100% of H_2O. For T_g, the stars at 0 mol% and 100 mol% H_2O show values that are fixed in the fit. Fitting parameters and root-mean-square error values are given in Table 2.

The steepness parameter m deviates between our model and literature fits (Figure 4) for the non-Arrhenian melt BasAnd2, which is already apparent in the fits themselves. m_d reported by Robert et al. (2013) is slightly higher than the value calculated here, and their m shows a steeper decrease with H_2O, resulting in an increasing deviation between the two models. For Pho1, our model formulation leads to lower values of m with H_2O compared to the fit by Giordano et al. (2009). The initial decrease is more pronounced than for BasAnd2. This behavior reflects that BasAnd2 has lower degree of polymerization, with the SM = 29.3 and x_{SiO_2} = 56.9 mol% (Table 2), an effect that is not clearly visible in the models from the literature.

In some cases—illustrated by Pho1 for our model (Figure 4f), but also apparent in some trends from the literature—m extrapolates to negative values at high H_2O content, which constitutes unphysical behavior. Such behavior should serve as warning against extrapolating models of melt viscosity far beyond the H_2O content actually measured in the experiments used for fitting.

Figure 5 shows a comparison of our fit calculation with RMSE = 0.17 against the measured viscosities as well as prediction of three general chemical viscosity models for these compositions (Duan, 2014; Giordano et al., 2008; Hui & Zhang, 2007). The model by Duan (2014) is the only viscosity model that accounts for the pressure effect on melt viscosity, which we fixed to 1 bar. Also, this model requires the partitioning of the total iron in FeO and Fe_2O_3. Here, for the melts for which iron partitioning was not provided, we assigned 1 / 2 of the total iron (always given as FeO_{tot}) as FeO and 1.11 / 2 as Fe_2O_3. The RMSE across all calculations is 1.95. The models by Giordano et al. (2008) and Hui and Zhang (2007) have RMSE values of 0.74 and 0.69 respectively. Table 2 documents the RMSE values for all three general chemical models and literature models for the individual compositions. Compared to the latter our model performs with comparable or better quality (Figure S5). However, previously published models differ in their formulations of H_2O dependence, while we use the same model for all melts (Equations 9–12). In the Supporting Information we provide an excel file to calculate viscosities for the melts referenced here.

Parameters c and d in Equation 9 obtained for six samples (Rhy8, Dac2, Tra3, Pho4, Pho5, Pho6) show strong deviations from the other values ($c > 19$ and $d < -24$, Table 2). This leads to unphysical extrapolations of T_g and—via Equation 12—m, that is, to an increase of T_g with H_2O content (Figure S4). Nevertheless, our model accurately reproduces the measured η data with RMSE = 0.09−0.35 for these six compositions. The anomalous behavior of T_g and m with H_2O appears to result from minimizing the residuals during the fit process. The unphysical extrapolation behavior serves as reminder to use our model—like any other model—not to extrapolate far beyond the experimental H_2O range.

6. Using DSC for Modeling Melt Viscosity

During viscometry experiments in the Hη regime volcanic melts can be subjected to nanostructural modification (i.e., crystallization and demixing) (Di Genova, Zandona, & Deubener, 2020), and DSC measurements provide an alternative route to obtain η data (e.g., Stabile et al., 2021). DSC measurements require a few mg of glass, which is exposed to $T > T_g$ for a few minutes only (Di Genova, Zandona, & Deubener, 2020; Stabile et al., 2021; Zheng et al., 2019). This is in stark contrast to experiments using micropenetration and parallel plate techniques that require large and double-polished samples (ideally with a thickness of ~ 3 mm) and expose the melt to $T > T_g$ for significantly longer periods of time (Douglas et al., 1965) which can lead to severe chemical and textural changes in anhydrous and hydrous samples (Bouhifd et al., 2004; Di Genova, Zandona, & Deubener, 2020; Liebske et al., 2003; Richet et al., 1996). However, only temperatures around T_g can be probed using DSC, leaving the Lη range unexplored, complicating η fitting. In Sections 4.2 and 4.3, we have explored the role of A for the η model, and found that using $A = -2.9$ (Zheng et al., 2011)—constraining the high T behavior—provides a systematic and good description of melt viscosity in the Lη range. Using $A = -2.9$ in the MYEGA fit and applying our description of H_2O dependence to DSC-derived η can therefore provide an alternative route to attain high-quality and reliable predictions.

6.1. Diopside: A Test Case

We test this approach for DSC-based data of a diopside melt (Di), an Fe-free system that is a good proxy of volcanic melt not prone to crystallization around T_g, and for which a large number of viscometry

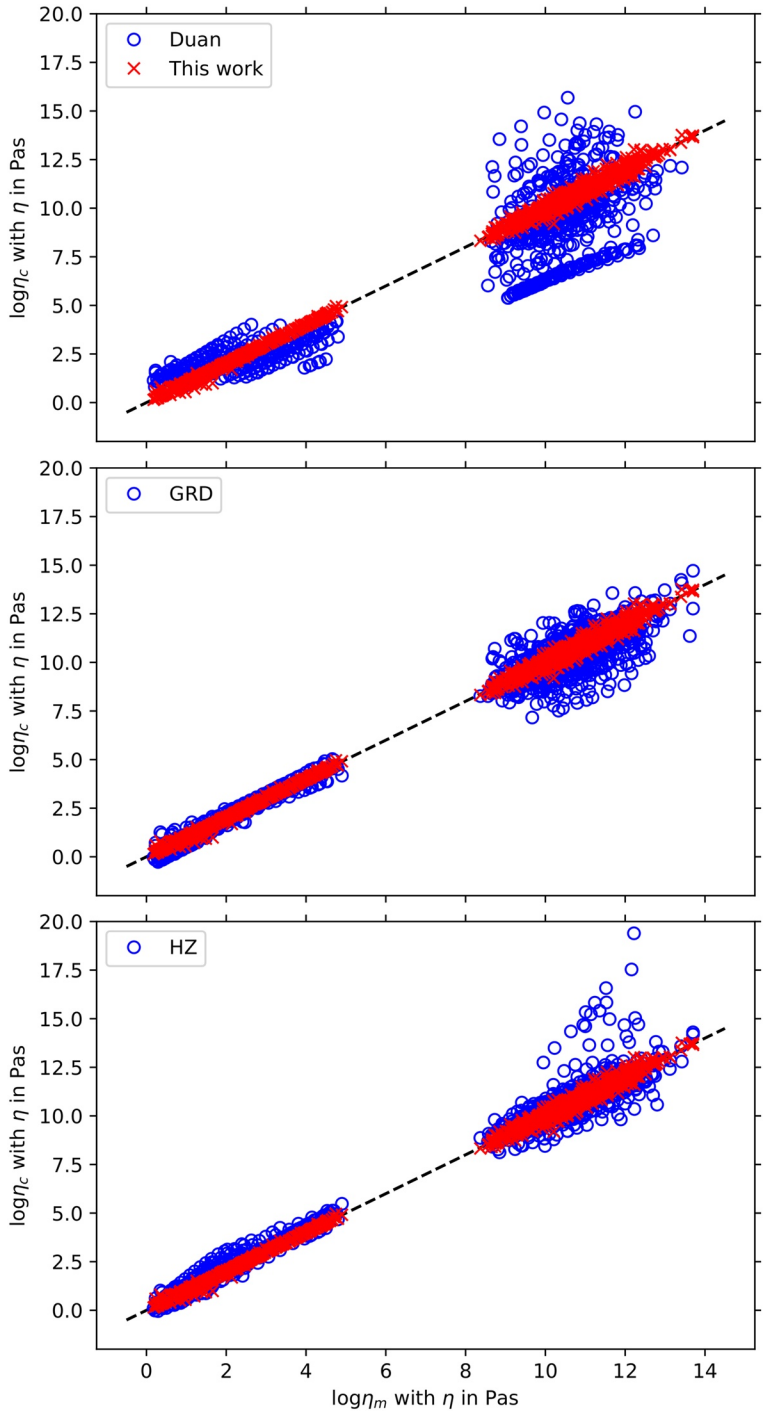

Figure 5. Viscosity values calculated using the hydrous fitting model (η_c) developed here (Equations 7 and 9–12) (red crosses) plotted against measured values (η_m) for the data from the 26 hydrous data sets (Table 2). As comparison, the chemical models by Duan (2014) (top), Giordano et al. (2008) (middle) and Hui and Zhang (2007) (bottom) are shown as blue circles. The solid line indicates the 1:1 correspondence. The root-mean-square error (RMSE) across all 1,251 datapoints for our model is RMSE = 0.17 log units. The general chemical models have RMSE values of 1.95, 0.74, and 0.69, respectively. Values of the fitting parameters and the RMSE for individual data sets and the respective references can be found in Table 2.

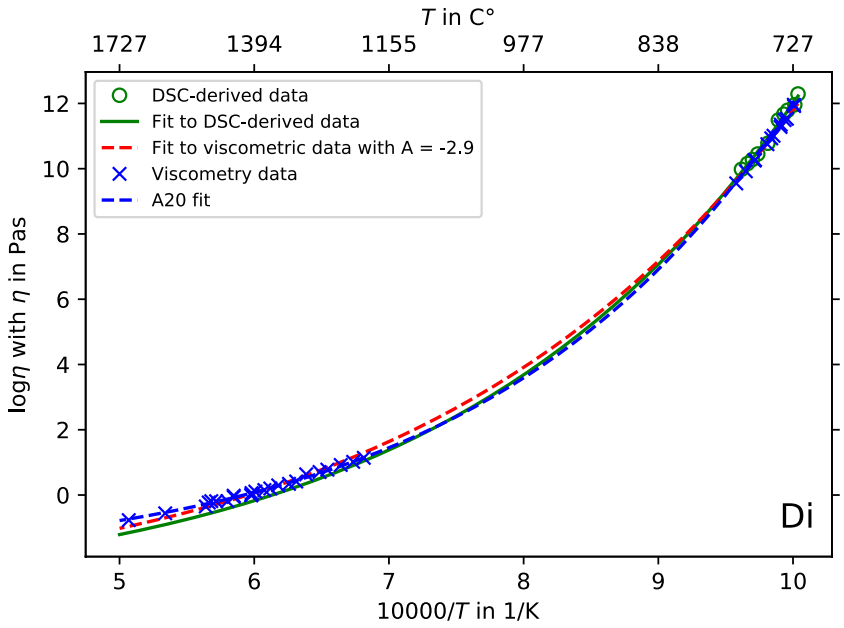

Figure 6. Comparison of differential scanning calorimetry (DSC)-derived viscosity data (green symbols) with viscometry measurements (blue symbols) for a diopside (Di). Our MYEGA model fit to the DSC-derived viscosities (green line) and to the viscometric measurements (red line) both use $A = -2.9$. The MYEGA fit to the viscometry data by Al-Mukadam et al. (2020) (A20) is shown by the blue line.

measurements in both Hη and Lη ranges as well as DSC data exist. Al-Mukadam et al. (2020) performed calorimetric measurements of Di and provided two rate-dependent characteristic T in the vicinity of T_g: T_{onset} marks the sudden drop in heat flow measured in DSC, and T_{peak} corresponds to the (endothermic) minimum of the heat flow undershoot of the glass transformation interval. T_{onset} and T_{peak} were measured at five heating rates, leading to 10 data points. We use the approach of Scherer (1984) to calculate η via

$$\log\eta(T_{onset/peak}) = K_{onset/peak} - log\ |q_{c,h}|, \tag{14}$$

where K is the chemically independent parallel shift factor and $|q_{c,h}|$ the heating rate in K s^{-1} for $T_{onset/peak}$ (Di Genova, Zandona, & Deubener, 2020).

Here we fit both the DSC-based values, that is, 10 data points with $\eta = 10^9 - 10^{12}$ Pa s (Figure 6) as well as the viscometric measurements compiled by Al-Mukadam et al. (2020), using the MYEGA expression (Equation 7) and assuming $A = -2.9$ (Zheng et al., 2011). Our fit and that by Al-Mukadam et al. (2020)—which leaves A free—to viscometry data show good agreement overall. The deviation at high T stems from the differing values in A. The MYEGA model based on DSC-derived viscosities (at Hη) predicts the Lη viscometry data well. Our approach shows that a predictive extrapolation from the Hη regime over more than 10 orders of magnitudes is reliably possible, spanning the entire η range relevant to volcanic eruptions.

6.2. Predicting Viscosities Using DSC

After testing this fitting approach on Di, we move to natural melts with fewer DSC data points and more complex oxide chemistry, which can lead to nanocrystallization even in the DSC experiments (Di Genova, Zandona, & Deubener, 2020). We compare the results from the fit to DSC-derived data with models that are based on viscometry measurement on melts of the same eruptions (Table 3): a Trachy-Basalt from Mt. Etna (Bas1-DSC), a Trachyte from Agnano-Monte Spina (Tra3-DSC), a Latite from Fondo Riccio (Lat-DSC), both located in the Phlegraean Fields, and a peralkaline Rhyolite from the island of Pantelleria (Rhy14-DSC), with Bas1, Tra3, Lat and Rhy14 (Table 2), the corresponding compositions with viscometry measurements. From the DSC measurements of Di Genova, Romano, Giordano, and Alletti (2014), we use selective data only, as even DSC upscans can induce nanocrystallization in volcanic melts (Di Genova, Zandona, &

Deubener, 2020). The presence of FeO-bearing nanocrystals in some samples has been suggested by Raman spectroscopy (Di Genova, Sicola, et al., 2017) and documented by transmission electron microscope (TEM) images for an anhydrous basalt from Mt. Etna following a DSC experiment (Di Genova, Zandona, & Deubener, 2020). We therefore take a conservative approach and use the characteristic temperatures from the first matching heating rate of 20 K min^{-1} to minimize the effect of possible alteration during the experiment. In addition to T_{onset} and T_{peak} described in Section 6.1, we also use T_{liquid} and its K factor, provided in Di Genova, Zandona, and Deubener (2020). With the 20 K min^{-1} heating rate, only data above T_g are generated, not constraining the slope (m) of η at 10^{12} Pa s well. To minimize the use of DSC data points beyond the initial heating, we use one more point, T_{onset} for 5 K min^{-1}, which provides T for $\log\eta = 12.3$.

Our model fit to the anhydrous DSC-derived data using $A = -2.9$ shows diverging behavior for Tra3, Bas1, and Lat in the Hη range when compared to η-models based on micropenetration measurements (Section 5) (Figure 7). A possible explanation for this discrepancy is nanostructure formation before or during micropenetration measurements at low T (Di Genova, Zandona, & Deubener, 2020). In particular, Di Genova, Zandona, and Deubener (2020) reported TEM images and Raman spectra of a nanolite-bearing Mt. Etna glass (i.e., Bas-1 composition) previously subjected to micropenetration and DSC measurements. They proved both scanning electron microscope and X-ray diffraction to be inconclusive in inferring the presence of nanolites due to their small size and low volume fraction. It was observed that with increasing nanocrystallization, viscosity increased toward values from melts of similar basaltic composition. Conversely, viscometry measurements in the Lη range are well predicted by the DSC-derived model. DSC-derived η for Rhy14 (Figure 7d) shows excellent agreement with micropenetration data (Di Genova et al., 2013), and agrees with their VFT model up to ~1200 °C. Contrary to the other three samples, a slight deviation can be observed between the DSC model prediction and the high-T viscometry measurements which can be traced to differences in m between the fits, DSC being better constrained at 10^{12} Pa s and showing a stronger non-Arrhenian behavior.

Similar to Di, η determined by viscometry at high T is well predicted by the extrapolation of the DSC-based description. This suggests that it is possible to accurately describe the Lη regime of volcanic melts using only measurements of the Hη range with (Zheng et al., 2011). This observation is further supported when considering the η differences between anhydrous viscometry- and DSC-based models at eruptive T of the melts that fall between the Hη and Lη region, with 900 °C for Lat (Cannatelli, 2012), 945 °C for Tra3, 1225 °C for Bas1, 750 °C for Rhy-14 (Di Genova et al., 2013), which therefore requires interpolation and extrapolation of η, respectively. Differences for the anhydrous compositions are small, ranging from 0.1 and 0.6 log units for Bas1 and Lat, respectively (Figure 8).

Now we extend our analysis to the hydrous DSC and viscometry measurements: for Lat-DSC, only DSC-based η values of one hydrous composition (5.71 mol%) are used from the data reported in Di Genova, Sicola, et al. (2017), for Bas1-DSC two hydrous compositions (5.24 mol% and 8.30 mol%); further data (3.6, 3.8 wt% for Bas1-DSC and 2.7, 3.8, 6.3 wt% for Lat-DSC) are excluded due to the presence of nanocrystals in the starting material (Di Genova, Sicola, et al., 2017).

The DSC-derived η of Tra3-DSC (Figure 7a) exhibits a T-dependence that our model describes well, and DSC- and viscometry-based models show good agreement for η in the ~ 4 mol% and 12–13 mol% H_2O ranges; they fit all experimental data well, with some deviations for 9.07 mol% H_2O. The difference in dependence of η on H_2O becomes apparent when the models are evaluated for 15.96 mol% H_2O: While the DSC-based model shows a further decrease of η with H_2O content at given T, the trend for the viscometry-based model reverses, with an unphysical increase. This behavior reflects the ill-behaved fitting parameters for Tra3 mentioned in Section 5 (Figure S4), reiterating the warning against using models for H_2O concentrations outside the range of fitting. This is also reflected in the change to a positive slope of Tra3 for ~ 12 mol% at eruptive T (Figure 8). Data for Bas1-DSC with 5.24 mol% and 8.30 mol% of H_2O do not provide a consistent picture in terms of $\eta - 1 / T$ (Figure 7b). The two low T and two high T points show different slope, and an offset. The two high T points represent the DSC measurements at T_{peak} and T_{liquid} for the 20 K min^{-1} heating rate, most likely reflecting nanocrystallization during the heating cycle in the DSC measurements, as mentioned above. Consequently, not all data can be fit with the same quality as for

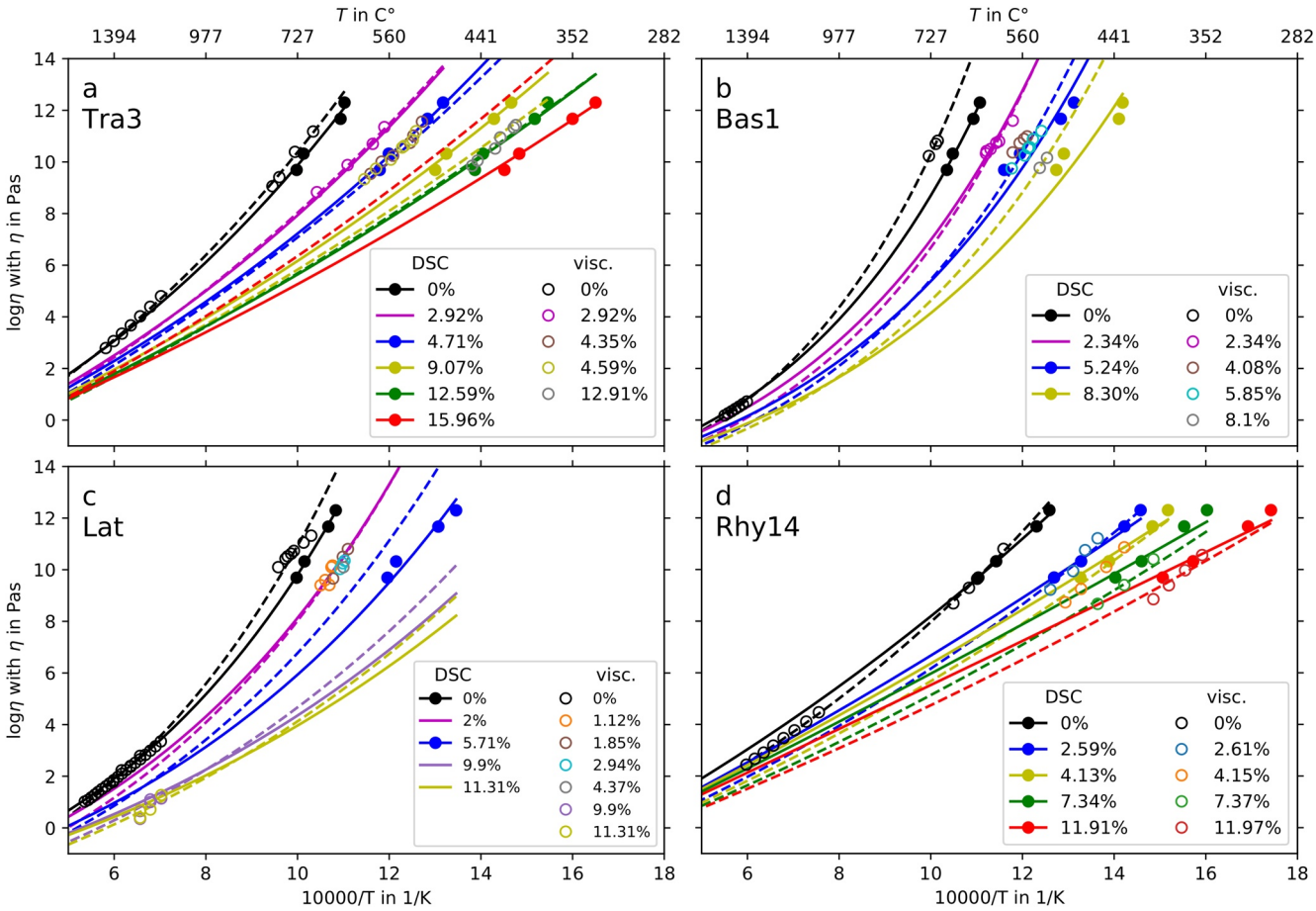

Figure 7. Comparison of viscosity data for Trachyte Tra3 (a), Basalt Bas1 (b), Latite Lat (c), and Rhyolite Rhy14 (d). Differential scanning calorimetry (DSC)-derived viscosities (filled circles) (Di Genova, Romano, Giordano, & Alletti, 2014) were obtained by using the shift factors K_i from Di Genova, Zandona, and Deubener (2020). Viscometry measurements (open circles) for Tra3 are from Romano et al. (2003), for Bas1 from Giordano and Dingwell (2003b), for Lat from Misiti et al. (2011), and for Rhy14 from Di Genova et al. (2013). Our MYEGA fits to the DSC data (solid lines) are calculated using $A = -2.9$. For comparison, our fits to the viscometric data from Section 5 are included (dashed lines). H_2O content indicated in the legends by solid lines only (DSC column) show curves for which the DSC model is evaluated, without DSC-derived η data available.

Tra3-DSC. Nevertheless, Bas1-DSC and Bas1 models agree well for ~ 5 mol% H_2O, and Bas1-DSC is able to predict the 2.34 mol% H_2O viscometric data accurately, without this water content being part of the DSC-based fit. At eruptive T, Bas1 and Bas1-DSC (Figure 8) show a consistent decrease of η with H_2O.

The Lat-DSC model deviates significantly for 5.71 mol% of H_2O from that of Lat (Figure 7c). This is caused by the η measurements of Misiti et al. (2011) showing little variation for 1.12 – 4.37 mol% H_2O, while the DSC-derived η values, based on the measurements with 5.71 mol% H_2O only, vary significantly over this range of water content. The Lat-DSC model reasonably reproduces viscometry-based η with a water content of 2 mol% (Misiti et al., 2011). Both models describe the Lη data at 10–11 mol% H_2O similarly well; for the viscometry-based Lat model they are used as input data, in Lat-DSC not. At eruptive T, the Lat-DSC model shows a well behaved, monotonically decreasing η with H_2O content (Figure 8), while Lat has a plateau at H_2O contents of ~ 2.5 mol% due to the clustering of similar η values for 1.12 – 4.37 mol% H_2O (Misiti et al., 2011). Consistent with the anhydrous data, viscometry measurements for Rhy14 show a steeper slope in $\eta - 1 / T$ compared to the DSC values for hydrous compositions (Figure 7d). Therefore the Rhy14 model predicts lower values in the Lη regime compared to Rhy14-DSC, and higher values in the Hη regime. At eruptive T, Rhy14 and Rhy14-DSC (Figure 8) show similar behavior, with the viscometric model generating lower η values; the difference between both models increases until it becomes approximately constant at ~ 7.5 mol% (2 wt%) with 0.8 – 0.9 log units.

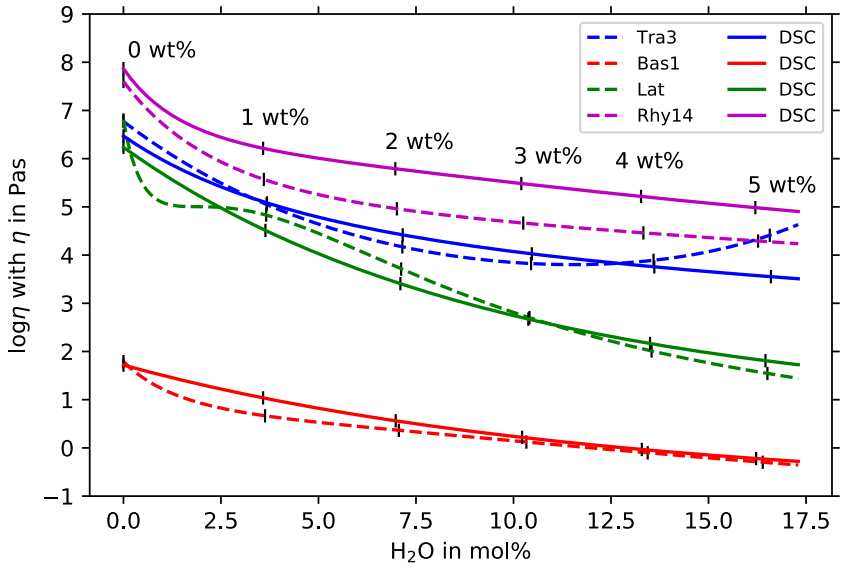

Figure 8. Comparison of H_2O dependence of differential scanning calorimetry (DSC) and viscometry derived models at eruptive T: 945 °C for Tra3, 1225 °C for Bas1, 900 °C for Lat, and 750 °C for Rhy14. Water content is given in mol%. The black ticks are set in 1 wt% intervals of H_2O concentration.

Our results for this set of examples indicate that hydrous DSC-derived η can be used to calibrate the model developed here (Equation 7 with $A = -2.9$ and Equations 9–12). Viscosity values of different H_2O concentration can not only be described well, but accurately predicted (Figure 7). Resulting η at eruptive T are well behaved with H_2O for all DSC-derived models. However, to fully validate this approach and explain the deviations between viscometry and DSC-derived models comprehensively, more DSC and viscometry measurements carried out on samples of equivalent compositions are necessary. As we have pointed out explicitly for Bas1, the formation of nanostructures appears to not only affect viscometry measurements, but also DSC experiments, albeit to a much smaller extent. Careful analysis of samples after experiments, for example, by Raman spectroscopy or TEM, is necessary to check for the formation of nanostructures (Di Genova, Zandona, & Deubener, 2020).

7. Conclusions

We present a new approach to fit the temperature and water dependence of viscosity for volcanic melts. It is based on a combination of the physically motivated MYEGA model (Mauro et al., 2009) (Equation 7) for an isochemical fit to anhydrous data and a two-component model (Schneider et al., 1997) to describe the influence of water. In the MYEGA model, the fitting parameters are the viscosity at infinite T ($A = \log\eta_\infty$), the glass transition temperature T_g, and the steepness factor m. In the two-component model, we formulate a dependence of T_g only between the endmembers of the anhydrous melt composition and that of water (Equations 9 and 10). For the dependence of m on water content, we derive an analytical expression dependent on T_g (Equation 12) and thereby on H_2O.

For a suite of 45 anhydrous melts (Table 1), we show that the MYEGA model describes the data comparably to—or better than—the more commonly used VFT fit. We further explore the performance of the MYEGA model by assuming a global constant value of $A = -2.9$ (Zheng et al., 2011); naturally, the misfit to the data increases, but the fits remain good overall. We also find that highly polymerized Arrhenian melts tend to yield smaller values of A due to the experimental inaccessibility of higher T measurements for these types of melts. For 26 data sets with both anhydrous and hydrous measurements, we apply the MYEGA model in combination with the H_2O-dependent description of T_g. We find that our model performs with comparable or better quality than various differing literature models (Table 2), including global chemical models. An

excel file to calculate viscosities of all melts considered here using our model is provided as Supporting Information.

We further investigate and fit viscosities derived from DSC which is an attractive experimental approach that avoids or reduces nanocrystallization and demixing of samples during the measurements compared to viscometric methods. The lack of low viscosity data due to DSC only probing T around T_g is compensated by using a constrained $A = -2.9$. For a small set of five examples (Table 3), we illustrate that such a fit extrapolates well to high T when compared to viscometry measurements. We apply the H_2O dependent model with $A = -2.9$ to hydrous DSC-derived viscosities, and find the model to show good fitting and predictive capabilities. Investigating these models at eruptive T also shows well behaved functions; viscosities monotonically decrease with H_2O content. This underlines the viability of determining η with DSC.

Since nanostructures have been shown to significantly influence η of volcanic melts (Di Genova, Brooker, et al., 2020; Di Genova, Kolzenburg, et al., 2017; Di Genova, Zandona, & Deubener, 2020), understanding and quantifying their impact on magma transport is an important task in physical volcanology. The characterization of samples exposed to DSC and viscometry measurements by Raman spectroscopy and transmission electron microscopy gives insight into the structural and textural impact of nanostructures. In combination with fitting the DSC-derived viscosities with $A = -2.9$ as well as viscometric measurements, this opens up the possibility to quantify the impact of nanostructure formation on the viscosity of volcanic melts. This in turn may improve our understanding of the eruptive dynamics of volcanoes.

Data Availability Statement

Data can be found in the cited references (Tables 1 and 3). An Excel file to compute viscosities with our model using fitting parameters of Table 2 is supplied as Supporting Information.

Acknowledgments
The authors acknowledge funding by Deutsche Forschungsgemeinschaft (DFG) projects DI 2751/2-1 and STE 1105/13-2. Open access funding enabled and organized by Projekt DEAL.

References

Adam, G., & Gibbs, J. H. (1965). On the temperature dependence of cooperative relaxation properties in glass-forming liquids. *The Journal of Chemical Physics*, *43*, 139–146. https://doi.org/10.1063/1.1696442

Alidibirov, M., Dingwell, D. B., Stevenson, R. J., Hess, K.-U., Webb, S. L., & Zinke, J. (1997). Physical properties of the 1980 Mount St. Helens cryptodome magma. *Bulletin of Volcanology*, *59*, 103–111. https://doi.org/10.1007/s004450050178

Al-Mukadam, R., Di Genova, D., Bornhöft, H., & Deubener, J. (2020). High rate calorimetry derived viscosity of oxide melts prone to crystallization. *Journal of Non-Crystalline Solids*, *536*, 119992. https://doi.org/10.1016/j.jnoncrysol.2020.119992

Angell, C. A. (1995). Formation of glasses from liquids and biopolymers. *Science*, *267*, 1924–1935. https://doi.org/10.1126/science.267.5206.1924

Angell, C. A. (1997). Entropy and fragility in supercooling liquids. *Journal of Research of the National Institute of Standards and Technology*, *102*, 171–185. https://doi.org/10.6028/jres.102.013

Angell, C. A., Ngai, K., McKenna, G. B., McMillan, P. F., & Martin, S. W. (2000). Relaxation in glassforming liquids and amorphous solids. *Journal of Applied Physics*, *88*, 3113–3157. https://doi.org/10.1063/1.1286035

Avramov, I., & Milchev, A. (1988). Effect of disorder on diffusion and viscosity in condensed systems. *Journal of Non-Crystalline Solids*, *104*, 253–260. https://doi.org/10.1016/0022-3093(88)90396-1

Bagdassarov, N. S., & Dingwell, D. B. (1992). A rheological investigation of vesicular rhyolite. *Journal of Volcanology and Geothermal Research*, *50*, 307–322. https://doi.org/10.1016/0377-0273(92)90099-Y

Baker, D. R. (1996). Granitic melt viscosities: Empirical and configurational entropy models for their calculation. *American Mineralogist*, *81*, 126–134. https://doi.org/10.2138/am-1996-1-216

Börjesson, L., Stevens, J. R., & Torell, L. M. (1987). Brillouin scattering studies of structural relaxations in poly (propylene glycol). *Polymer*, *28*, 1803–1808. https://doi.org/10.1016/0032-3861(87)90281-3

Bottinga, Y., & Weill, D. F. (1972). The viscosity of magmatic silicate liquids: A model calculation. *American Journal of Science*, *272*, 438–475. https://doi.org/10.2475/ajs.272.5.438

Bouhifd, M. A., Richet, P., Besson, P., Roskosz, M., & Ingrin, J. (2004). Redox state, microstructure and viscosity of a partially crystallized basalt melt. *Earth and Planetary Science Letters*, *218*, 31–44. https://doi.org/10.1016/S0012-821X(03)00641-1

Bouhifd, M. A., Whittington, A., Roux, J., & Richet, P. (2006). Effect of water on the heat capacity of polymerized aluminosilicate glasses and melts. *Geochimica et Cosmochimica Acta*, *70*, 711–722. https://doi.org/10.1016/j.gca.2005.09.012

Cannatelli, C. (2012). Understanding magma evolution at Campi Flegrei (Campania, Italy) volcanic complex using melt inclusions and phase equilibria. *Mineralogy and Petrology*, *104*, 29–42. https://doi.org/10.1007/s00710-011-0182-6

Caricchi, L., Burlini, L., Ulmer, P., Gerya, T., Vassalli, M., & Papale, P. (2007). Non-Newtonian rheology of crystal-bearing magmas and implications for magma ascent dynamics. *Earth and Planetary Science Letters*, *264*, 402–419. https://doi.org/10.1016/j.epsl.2007.09.032

Cassidy, M., Manga, M., Cashman, K., & Bachmann, O. (2018). Controls on explosive-effusive volcanic eruption styles. *Nature Communications*, *9*, 2839. https://doi.org/10.1038/s41467-018-05293-3

Chevrel, M. O., Cimarelli, C., de Biasi, L., Hanson, J. B., Lavallée, Y., Arzilli, F., & Dingwell, D. B. (2015). Viscosity measurements of crystallizing andesite from Tungurahua volcano (Ecuador). *Geochemistry, Geophysics, Geosystems*, *16*, 870–889. https://doi.org/10.1002/2014GC005661

Chevrel, M. O., Giordano, D., Potuzak, M., Courtial, P., & Dingwell, D. B. (2013). Physical properties of $CaAl_2Si_2O_8$–$CaMgSi_2O_6$–FeO–Fe_2O_3 melts: Analogues for extra-terrestrial basalt. *Chemical Geology*, *346*, 93–105. https://doi.org/10.1016/j.chemgeo.2012.09.004

Colucci, S., & Papale, P. (2021). Deep magma transport control on the size and evolution of explosive volcanic eruptions. *Frontiers in Earth Science*, *9*, 436. https://doi.org/10.3389/feart.2021.681083

Cordonnier, B., Hess, K.-U., Lavallee, Y., & Dingwell, D. B. (2009). Rheological properties of dome lavas: Case study of Unzen volcano. *Earth and Planetary Science Letters*, *279*, 263–272. https://doi.org/10.1016/j.epsl.2009.01.014

Costa, A., Caricchi, L., & Bagdassarov, N. (2009). A model for the rheology of particle-bearing suspensions and partially molten rocks. *Geochemistry, Geophysics, Geosystems*, *10*. https://doi.org/10.1029/2008GC002138

Davì, M., Behrens, H., Vetere, F., & De Rosa, R. (2009). The viscosity of latitic melts from Lipari (Aeolian Islands, Italy): Inference on mixing–mingling processes in magmas. *Chemical Geology*, *259*, 89–97. https://doi.org/10.1016/j.chemgeo.2008.10.009

Di Genova, D., Brooker, R. A., Mader, H. M., Drewitt, J. W. E., Longo, A., Deubener, J., et al. (2020). In situ observation of nanolite growth in volcanic melt: A driving force for explosive eruptions. *Science Advances*, *6*, eabb0413. https://doi.org/10.1126/sciadv.abb0413

Di Genova, D., Kolzenburg, S., Wiesmaier, S., Dallanave, E., Neuville, D. R., Hess, K.-U., & Dingwell, D. B. (2017). A compositional tipping point governing the mobilization and eruption style of rhyolitic magma. *Nature*, *552*, 235–238. https://doi.org/10.1038/nature24488

Di Genova, D., Romano, C., Alletti, M., Misiti, V., & Scarlato, P. (2014). The effect of CO_2 and H_2O on Etna and Fondo Riccio (Phlegrean Fields) liquid viscosity, glass transition temperature and heat capacity. *Chemical Geology*, *377*, 72–86. https://doi.org/10.1016/j.chemgeo.2014.04.001

Di Genova, D., Romano, C., Giordano, D., & Alletti, M. (2014). Heat capacity, configurational heat capacity and fragility of hydrous magmas. *Geochimica et Cosmochimica Acta*, *142*, 314–333. https://doi.org/10.1016/j.gca.2014.07.012

Di Genova, D., Romano, C., Hess, K.-U., Vona, A., Poe, B. T., Giordano, D., et al. (2013). The rheology of peralkaline rhyolites from Pantelleria Island. *Journal of Volcanology and Geothermal Research*, *249*, 201–216. https://doi.org/10.1016/j.jvolgeores.2012.10.017

Di Genova, D., Sicola, S., Romano, C., Vona, A., Fanara, S., & Spina, L. (2017). Effect of iron and nanolites on Raman spectra of volcanic glasses: A reassessment of existing strategies to estimate the water content. *Chemical Geology*, *475*, 76–86. https://doi.org/10.1016/j.chemgeo.2017.10.035

Di Genova, D., Zandona, A., & Deubener, J. (2020). Unravelling the effect of nano-heterogeneity on the viscosity of silicate melts: Implications for glass manufacturing and volcanic eruptions. *Journal of Non-Crystalline Solids*, *545*, 120248. https://doi.org/10.1016/j.jnoncrysol.2020.120248

Dingwell, D. B. (1996). Volcanic dilemma—Flow or blow? *Science*, *273*, 1054–1055. https://doi.org/10.1126/science.273.5278.1054

Dingwell, D. B., Courtial, P., Giordano, D., & Nichols, A. R. L. (2004). Viscosity of peridotite liquid. *Earth and Planetary Science Letters*, *226*, 127–138. https://doi.org/10.1016/j.epsl.2004.07.017

Dingwell, D. B., Hess, K.-U., & Romano, C. (1998a). Extremely fluid behavior of hydrous peralkaline rhyolites. *Earth and Planetary Science Letters*, *158*, 31–38. https://doi.org/10.1016/S0012-821X(98)00046-6

Dingwell, D. B., Hess, K.-U., & Romano, C. (1998b). Viscosity data for hydrous peraluminous granitic melts; comparison with a metaluminous model. *American Mineralogist*, *83*, 236–239. https://doi.org/10.2138/am-1998-3-406

Dingwell, D. B., Romano, C., & Hess, K.-U. (1996). The effect of water on the viscosity of a haplogranitic melt under PTX conditions relevant to silicic volcanism. *Contributions to Mineralogy and Petrology*, *124*, 19–28. https://doi.org/10.1007/s004100050170

Dingwell, D. B., & Webb, S. L. (1989). Structural relaxation in silicate melts and non-Newtonian melt rheology in geologic processes. *Physics and Chemistry of Minerals*, *16*, 508–516. https://doi.org/10.1007/BF00197020

Dobson, D. P., Jones, A. P., Rabe, R., Sekine, T., Kurita, K., Taniguchi, T., et al. (1996). In-situ measurement of viscosity and density of carbonate melts at high pressure. *Earth and Planetary Science Letters*, *143*, 207–215. https://doi.org/10.1016/0012-821X(96)00139-2

Douglas, R. W., Armstrong, W. L., Edward, J. P., & Hall, D. (1965). A penetration viscometer. *Glass Technology*, *6*, 52–55.

Duan, X. (2014). A model for calculating the viscosity of natural iron-bearing silicate melts over a wide range of temperatures, pressures, oxygen fugacities, and compositions. *American Mineralogist*, *99*, 2378–2388. https://doi.org/10.2138/am-2014-4841

Fujimori, H., & Oguni, M. (1995). Correlation index $(T_{g,\alpha}-T_{g,\beta})/T_{g,\alpha}$ and activation energy ratio $\Delta\epsilon_{a,\alpha}/\Delta\epsilon_{a,\beta}$ parameters characterizing the structure of liquid and glass. *Solid State Communications*, *94*, 157–162. https://doi.org/10.1016/0038-1098(94)00851-5

Fulcher, G. S. (1925). Analysis of recent measurements of the viscosity of glasses. *Journal of the American Ceramic Society*, *8*, 339–355. https://doi.org/10.1111/j.1151-2916.1925.tb16731.x

Gibbs, J. H., & DiMarzio, E. A. (1958). Nature of the glass transition and the glassy state. *The Journal of Chemical Physics*, *28*, 373–383. https://doi.org/10.1063/1.1744141

Giordano, D., Ardia, P., Romano, C., Dingwell, D. B., Di Muro, A., Schmidt, M. W., et al. (2009). The rheological evolution of alkaline Vesuvius magmas and comparison with alkaline series from the Phlegrean Fields, Etna, Stromboli and Teide. *Geochimica et Cosmochimica Acta*, *73*, 6613–6630. https://doi.org/10.1016/j.gca.2009.07.033

Giordano, D., & Dingwell, D. B. (2003a). Non-Arrhenian multicomponent melt viscosity: A model. *Earth and Planetary Science Letters*, *208*, 337–349. https://doi.org/10.1016/S0012-821X(03)00042-6

Giordano, D., & Dingwell, D. B. (2003b). Viscosity of hydrous Etna basalt: Implications for Plinian-style basaltic eruptions. *Bulletin of Volcanology*, *65*, 8–14. https://doi.org/10.1007/s00445-002-0233-2

Giordano, D., Dingwell, D. B., & Romano, C. (2000). Viscosity of a Teide phonolite in the welding interval. *Journal of Volcanology and Geothermal Research*, *103*, 239–245. https://doi.org/10.1016/S0377-0273(00)00226-2

Giordano, D., Mangiacapra, A., Potuzak, M., Russell, J. K., Romano, C., Dingwell, D. B., & Di Muro, A. (2006). An expanded non-Arrhenian model for silicate melt viscosity: A treatment for metaluminous, peraluminous and peralkaline liquids. *Chemical Geology*, *229*, 42–56. https://doi.org/10.1016/j.chemgeo.2006.01.007

Giordano, D., Romano, C., Papale, P., & Dingwell, D. B. (2004). The viscosity of trachytes, and comparison with basalts, phonolites, and rhyolites. *Chemical Geology*, *213*, 49–61. https://doi.org/10.1016/j.chemgeo.2004.08.032

Giordano, D., & Russell, J. K. (2017). The heat capacity of hydrous multicomponent natural melts and glasses. *Chemical Geology*, *461*, 96–103. https://doi.org/10.1016/j.chemgeo.2016.08.036

Giordano, D., Russell, J. K., & Dingwell, D. B. (2008). Viscosity of magmatic liquids: A model. *Earth and Planetary Science Letters*, *271*, 123–134. https://doi.org/10.1016/j.epsl.2008.03.038

Gonnermann, H. M., & Manga, M. (2007). The fluid mechanics inside a volcano. *Annual Review of Fluid Mechanics*, *39*, 321–356. https://doi.org/10.1146/annurev.fluid.39.050905.110207

Gonnermann, H. M., & Manga, M. (2013). Dynamics of magma ascent in the volcanic conduit. In *Modeling volcanic processes: The physics and mathematics of volcanism* (pp. 55–84).

Gordon, M., & Taylor, J. S. (1952). Ideal copolymers and the second-order transition of synthetic rubber. I. Non-crystalline copolymers. *Journal of Applied Chemistry*, *3*, 493–500. https://doi.org/10.1002/jctb.5010020901
Hamilton, D. L., Burnham, C. W., & Osborn, E. F. (1964). The solubility of water and effects of oxygen fugacity and water content on crystallization in mafic magmas. *Journal of Petrology*, *5*, 21–39. https://doi.org/10.1093/petrology/5.1.21
Hecksher, T., Nielsen, A. I., Olsen, N. B., & Dyre, J. C. (2008). Little evidence for dynamic divergences in ultraviscous molecular liquids. *Nature Physics*, *4*, 737–741. https://doi.org/10.1038/nphys1033
Hess, K.-U., & Dingwell, D. B. (1996). Viscosities of hydrous leucogranitic melts: A non-Arrhenian model. *American Mineralogist*, *81*, 1297–1300. https://doi.org/10.2138/am-1996-9-1031
Hess, K.-U., Dingwell, D. B., Gennaro, C., & Mincione, V. (2001). Viscosity–temperature behaviour of dry melts in the Qz–Ab–Or system. *Chemical Geology*, *174*, 133–142. https://doi.org/10.1016/S0009-2541(00)00312-0
Hess, K.-U., Dingwell, D. B., & Webb, S. L. (1995). The influence of excess alkalis on the viscosity of a haplogranitic melt. *American Mineralogist*, *80*, 297–304. https://doi.org/10.2138/am-1995-3-411
Hui, H., & Zhang, Y. (2007). Toward a general viscosity equation for natural anhydrous and hydrous silicate melts. *Geochimica et Cosmochimica Acta*, *71*, 403–416. https://doi.org/10.1016/j.gca.2006.09.003
Ishibashi, H., & Sato, H. (2007). Viscosity measurements of subliquidus magmas: Alkali olivine basalt from the Higashi-Matsuura district, Southwest Japan. *Journal of Volcanology and Geothermal Research*, *160*, 223–238. https://doi.org/10.1016/j.jvolgeores.2006.10.001
Kohl, I., Bachmann, L., Mayer, E., Hallbrucker, A., & Loerting, T. (2005). Glass transition in hyperquenched water? *Nature*, *435*, E1. https://doi.org/10.1038/nature03707
Kolzenburg, S., Di Genova, D., Giordano, D., Hess, K.-U., & Dingwell, D. B. (2018). The effect of oxygen fugacity on the rheological evolution of crystallizing basaltic melts. *Earth and Planetary Science Letters*, *487*, 21–32. https://doi.org/10.1016/j.epsl.2018.01.023
Laughlin, W. T., & Uhlmann, D. R. (1972). Viscous flow in simple organic liquids. *Journal of Physical Chemistry*, *76*, 2317–2325. https://doi.org/10.1021/j100660a023
Le Bas, M. J., Le Maitre, R. W., Streckeisen, A., & Zanettin, B. (1986). A chemical classification of volcanic rocks based on the total alkali-silica diagram. *Journal of Petrology*, *27*, 745–750. https://doi.org/10.1093/petrology/27.3.745
Lejeune, A. M., Bottinga, Y., Trull, T. W., & Richet, P. (1999). Rheology of bubble-bearing magmas. *Earth and Planetary Science Letters*, *166*, 71–84. https://doi.org/10.1016/S0012-821X(98)00278-7
Liebske, C., Behrens, H., Holtz, F., & Lange, R. A. (2003). The influence of pressure and composition on the viscosity of andesitic melts. *Geochimica et Cosmochimica Acta*, *67*, 473–485. https://doi.org/10.1016/S0016-7037(02)01139-0
Liebske, C., Schmickler, B., Terasaki, H., Poe, B. T., Suzuki, A., Funakoshi, K., et al. (2005). Viscosity of peridotite liquid up to 13 GPa: Implications for magma ocean viscosities. *Earth and Planetary Science Letters*, *240*, 589–604. https://doi.org/10.1016/j.epsl.2005.10.004
Llewellin, E. W., & Manga, M. (2005). Bubble suspension rheology and implications for conduit flow. *Journal of Volcanology and Geothermal Research*, *143*, 205–217. https://doi.org/10.1016/j.jvolgeores.2004.09.018
Mader, H. M., Llewellin, E. W., & Mueller, S. P. (2013). The rheology of two-phase magmas: A review and analysis. *Journal of Volcanology and Geothermal Research*, *257*, 135–158. https://doi.org/10.1016/j.jvolgeores.2013.02.014
Manga, M., Castro, J., Cashman, K. V., & Loewenberg, M. (1998). Rheology of bubble-bearing magmas. *Journal of Volcanology and Geothermal Research*, *87*, 15–28. https://doi.org/10.1016/S0377-0273(98)00091-2
Markl, G., Marks, M. A. W., & Frost, B. R. (2010). On the controls of oxygen fugacity in the generation and crystallization of peralkaline melts. *Journal of Petrology*, *51*, 1831–1847. https://doi.org/10.1093/petrology/egq040
Marzocchi, W., Newhall, C., & Woo, G. (2012). The scientific management of volcanic crises. *Journal of Volcanology and Geothermal Research*, *247*, 181–189. https://doi.org/10.1016/j.jvolgeores.2012.08.016
Mastin, L. G., Guffanti, M., Servranckx, R., Webley, P., Barsotti, S., Dean, K., et al. (2009). A multidisciplinary effort to assign realistic source parameters to models of volcanic ash-cloud transport and dispersion during eruptions. *Journal of Volcanology and Geothermal Research*, *186*, 10–21. https://doi.org/10.1016/j.jvolgeores.2009.01.008
Mauro, J. C., Yue, Y., Ellison, A. J., Gupta, K., & Allan, D. C. (2009). Viscosity of glass-forming liquids. *Proceedings of the National Academy of Sciences of the United States of America*, *106*, 19780–19784. https://doi.org/10.1073/pnas.0911705106
Misiti, V., Vetere, F., Freda, C., Scarlato, P., Behrens, H., Mangiacapra, A., & Dingwell, D. B. (2011). A general viscosity model of Campi Flegrei (Italy) melts. *Chemical Geology*, *290*, 50–59. https://doi.org/10.1016/j.chemgeo.2011.08.010
Misiti, V., Vetere, F., Mangiacapra, A., Behrens, H., Cavallo, A., Scarlato, P., & Dingwell, D. B. (2009). Viscosity of high-K basalt from the 5th April 2003 Stromboli paroxysmal explosion. *Chemical Geology*, *260*, 278–285. https://doi.org/10.1016/j.chemgeo.2008.12.023
Mueller, S., Llewellin, E. W., & Mader, H. M. (2010). The rheology of suspensions of solid particles. *Proceedings of the Royal Society A: Mathematical, Physical and Engineering Sciences*, *466*, 1201–1228. https://doi.org/10.1098/rspa.2009.0445
Mysen, B. O. (1988). *Structure and properties of silicate melts*. Elsevier.
Neuville, D. R., Courtial, P., Dingwell, D. B., & Richet, P. (1993). Thermodynamic and rheological properties of rhyolite and andesite melts. *Contributions to Mineralogy and Petrology*, *113*, 572–581. https://doi.org/10.1007/BF00698324
Ni, H., Hui, H., & Steinle-Neumann, G. (2015). Transport properties of silicate melts. *Reviews of Geophysics*, *53*, 715–744. https://doi.org/10.1002/2015RG000485
Norton, G., & Pinkerton, H. (1997). Rheological properties of natrocarbonatite lavas from Oldoinyo Lengai, Tanzania. *European Journal of Mineralogy*, *9*, 351–364. https://doi.org/10.1127/ejm/9/2/0351
Ongaro, T. E., Neri, A., Menconi, G., Vitturi, M., Marianelli, P., Cavazzoni, C., et al. (2008). Transient 3D numerical simulations of column collapse and pyroclastic density current scenarios at Vesuvius. *Journal of Volcanology and Geothermal Research*, *178*, 378–396. https://doi.org/10.1016/j.jvolgeores.2008.06.036
Papale, P. (1999). Strain-induced magma fragmentation in explosive eruptions. *Nature*, *397*, 425–428. https://doi.org/10.1038/17109
Persikov, E. S. (1998). The viscosity of model and magmatic melts under P–T-parameters of the Earth's crust and upper mantle. *Russian Geology and Geophysics*, *39*, 1780–1792.
Phan-Thien, N., & Pham, D. C. (1997). Differential multiphase models for polydispersed suspensions and particulate solids. *Journal of Non-Newtonian Fluid Mechanics*, *72*, 305–318. https://doi.org/10.1016/S0377-0257(97)90002-1
Pistone, M., Caricchi, L., Ulmer, P., Burlini, L., Ardia, P., Reusser, E., et al. (2012). Deformation experiments of bubble-and crystal-bearing magmas: Rheological and microstructural analysis. *Journal of Geophysical Research*, *117*, B05208. https://doi.org/10.1029/2011JB008986
Pistone, M., Cordonnier, B., Ulmer, P., & Caricchi, L. (2016). Rheological flow laws for multiphase magmas: An empirical approach. *Journal of Volcanology and Geothermal Research*, *321*, 158–170. https://doi.org/10.1016/j.jvolgeores.2016.04.029
Richet, P. (1984). Viscosity and configurational entropy of silicate melts. *Geochimica et Cosmochimica Acta*, *48*, 471–483. https://doi.org/10.1016/0016-7037(84)90275-8

Richet, P. (1987). Heat capacity of silicate glasses. *Chemical Geology*, *62*, 111–124. https://doi.org/10.1016/0009-2541(87)90062-3
Richet, P., Lejeune, A.-M., Holtz, F., & Roux, J. (1996). Water and the viscosity of andesite melts. *Chemical Geology*, *128*, 185–197. https://doi.org/10.1016/0009-2541(95)00172-7
Robert, G. (2014). *The effects of volatiles on the viscosity and heat capacity of calc-alkaline basaltic and basaltic andesite liquids* (Doctoral Dissertation). University of Missouri.
Robert, G., Knipping, J. L., Scherbarth, S., Robertson, T. E., Stechern, A., Behrens, H., & Whittington, A. G. (2015). Heat capacity and viscosity of basaltic melts with H_2O±F±CO_2. *Chemical Geology*, *418*, 51–65. https://doi.org/10.1016/j.chemgeo.2014.07.015
Robert, G., Whittington, A., Stechern, A., & Behrens, H. (2013). The effect of water on the viscosity of a synthetic calc-alkaline basaltic andesite. *Chemical Geology*, *346*, 135–148. https://doi.org/10.1016/j.chemgeo.2012.10.004
Robert, G., Whittington, A. G., Stechern, A., & Behrens, H. (2014). Heat capacity of hydrous basaltic glasses and liquids. *Journal of Non-Crystalline Solids*, *390*, 19–30. https://doi.org/10.1016/j.jnoncrysol.2014.02.011
Romano, C., Giordano, D., Papale, P., Mincione, V., Dingwell, D. B., & Rosi, M. (2003). The dry and hydrous viscosities of alkaline melts from Vesuvius and Phlegrean Fields. *Chemical Geology*, *202*, 23–38. https://doi.org/10.1016/S0009-2541(03)00208-0
Romine, W. L., & Whittington, A. G. (2015). A simple model for the viscosity of Rhyolites as a function of temperature, pressure and water content. *Geochimica et Cosmochimica Acta*, *170*, 281–300. https://doi.org/10.1016/j.gca.2015.08.009
Russell, J. K., & Giordano, D. (2017). Modelling configurational entropy of silicate melts. *Chemical Geology*, *461*, 140–151. https://doi.org/10.1016/j.chemgeo.2016.07.019
Russell, J. K., Giordano, D., & Dingwell, D. B. (2003). High–temperature limits on viscosity of non–Arrhenian silicate melts. *American Mineralogist*, *88*, 1390–1394. https://doi.org/10.2138/am-2003-8-924
Sato, H. (2005). Viscosity measurement of subliquidus magmas: 1707 basalt of Fuji volcano. *Journal of Mineralogical and Petrological Sciences*, *100*, 133–142. https://doi.org/10.2465/jmps.100.133
Scherer, G. W. (1984). Use of the Adam-Gibbs equation in the analysis of structural relaxation. *Journal of the American Ceramic Society*, *67*, 504–511. https://doi.org/10.1111/j.1151-2916.1984.tb19643.x
Scherer, G. W. (1992). Editorial comments on a paper by Gordon S. Fulcher. *Journal of the American Ceramic Society*, *75*, 1060–1062. https://doi.org/10.1111/j.1151-2916.1992.tb05537.x
Schmelzer, J. W. P., Abyzov, A. S., Fokin, V. M., & Schick, C. (2018). Kauzmann paradox and the crystallization of glass-forming melts. *Journal of Non-Crystalline Solids*, *501*, 21–35. https://doi.org/10.1016/j.jnoncrysol.2017.11.045
Schneider, H. A., Rieger, J., & Penzel, E. (1997). The glass transition temperature of random copolymers: 2. Extension of the Gordon Taylor equation for asymmetric T_g vs composition curves. *Polymer*, *38*, 1323–1337. https://doi.org/10.1016/S0032-3861(96)00652-0
Sehlke, A., Whittington, A., Robert, B., Harris, A., Gurioli, L., & Médard, E. (2014). Pahoehoe toaa transition of Hawaiian lavas: An experimental study. *Bulletin of Volcanology*, *76*, 876. https://doi.org/10.1007/s00445-014-0876-9
Sehlke, A., & Whittington, A. G. (2016). The viscosity of planetary tholeiitic melts: A configurational entropy model. *Geochimica et Cosmochimica Acta*, *191*, 277–299. https://doi.org/10.1016/j.gca.2016.07.027
Shaw, H. R. (1972). Viscosities of magmatic silicate liquids: An empirical method of prediction. *American Journal of Science*, *272*, 870–893. https://doi.org/10.2475/ajs.272.9.870
Stabile, P., Sicola, S., Giuli, G., Paris, E., Carroll, M. R., Deubener, J., & Di Genova, D. (2021). The effect of iron and alkali on the nanocrystal-free viscosity of volcanic melts: A combined Raman spectroscopy and DSC study. *Chemical Geology*, *559*, 119991. https://doi.org/10.1016/j.chemgeo.2020.119991
Stabile, P., Webb, S., Knipping, J. L., Behrens, H., Paris, E., & Giuli, G. (2016). Viscosity of pantelleritic and alkali-silicate melts: Effect of Fe redox state and Na/(Na+K) ratio. *Chemical Geology*, *442*, 73–82. https://doi.org/10.1016/j.chemgeo.2016.09.003
Stagno, V., Stopponi, V., Kono, Y., Manning, C. E., & Irifune, T. (2018). Experimental determination of the viscosity of Na_2CO_3 melt between 1.7 and 4.6 GPa at 1200–1700°C: Implications for the rheology of carbonatite magmas in the Earth's upper mantle. *Chemical Geology*, *501*, 19–25. https://doi.org/10.1016/j.chemgeo.2018.09.036
Stebbins, J. F., Carmichael, I. S. E., & Moret, L. K. (1984). Heat capacities and entropies of silicate liquids and glasses. *Contributions to Mineralogy and Petrology*, *86*, 131–148. https://doi.org/10.1007/BF00381840
Stein, D. J., & Spera, F. J. (2002). Shear viscosity of rhyolite-vapor emulsions at magmatic temperatures by concentric cylinder rheometry. *Journal of Volcanology and Geothermal Research*, *113*, 243–258. https://doi.org/10.1016/S0377-0273(01)00260-8
Stillinger, F. H. (1988). Supercooled liquids, glass transitions, and the Kauzmann paradox. *The Journal of Chemical Physics*, *88*, 7818–7825. https://doi.org/10.1063/1.454295
Tammann, G., & Hesse, W. (1926). Die Abhängigkeit der Viskosität von der Temperatur bei unterkühlten Flüssigkeiten. *Zeitschrift für Anorganische und Allgemeine Chemie*, *156*, 245–257. https://doi.org/10.1002/zaac.19261560121
Toplis, M. J. (1998). Energy barriers to viscous flow and the prediction of glass transition temperatures of molten silicates. *American Mineralogist*, *83*, 480–490. https://doi.org/10.2138/am-1998-5-608
Toplis, M. J., & Carroll, M. (1995). An experimental study of the influence of oxygen fugacity on Fe-Ti oxide stability, phase relations, and mineral—Melt equilibria in ferro-basaltic systems. *Journal of Petrology*, *36*, 1137–1170. https://doi.org/10.1093/petrology/36.5.1137
Truby, J. M., Mueller, S. P., Llewellin, E. W., & Mader, H. M. (2015). The rheology of three-phase suspensions at low bubble capillary number. *Proceedings of the Royal Society A: Mathematical, Physical & Engineering Sciences*, *471*, 20140557. https://doi.org/10.1098/rspa.2014.0557
Vetere, F., Behrens, H., Holtz, F., & Neuville, D. R. (2006). Viscosity of andesitic melts—New experimental data and a revised calculation model. *Chemical Geology*, *228*, 233–245. https://doi.org/10.1016/j.chemgeo.2005.10.009
Vetere, F., Behrens, H., Misiti, V., Ventura, G., Holtz, F., De Rosa, R., & Deubener, J. (2007). The viscosity of shoshonitic melts (Vulcanello Peninsula, Aeolian Islands, Italy): Insight on the magma ascent in dikes. *Chemical Geology*, *245*, 89–102. https://doi.org/10.1016/j.chemgeo.2007.08.002
Vetere, F., Behrens, H., Schuessler, J. A., Holtz, F., Misiti, V., & Borchers, L. (2008). Viscosity of andesite melts and its implication for magma mixing prior to Unzen 1991–1995 eruption. *Journal of Volcanology and Geothermal Research*, *175*, 208–217. https://doi.org/10.1016/j.jvolgeores.2008.03.028
Vetere, F., Sato, H., Ishibashi, H., De Rosa, R., & Donato, P. (2013). Viscosity changes during crystallization of a shoshonitic magma: New insights on lava flow emplacement. *Journal of Mineralogical and Petrological Sciences*, *108*, 144–160. https://doi.org/10.2465/jmps.120724
Vogel, H. (1921). Das Temperaturabhängigkeitsgesetz der Viskosität von Flüssigkeiten. *Physikalische Zeitschrift*, *22*, 645–646.
Vona, A., Di Piazza, A., Nicotra, E., Romano, C., Viccaro, M., & Giordano, G. (2017). The complex rheology of megacryst-rich magmas: The case of the mugearitic "cicirara" lavas of Mt. Etna volcano. *Chemical Geology*, *458*, 48–67. https://doi.org/10.1016/j.chemgeo.2017.03.029

Vona, A., Romano, C., Dingwell, D. B., & Giordano, D. (2011). The rheology of crystal-bearing basaltic magmas from Stromboli and Etna. *Geochimica et Cosmochimica Acta*, *75*, 3214–3236. https://doi.org/10.1016/j.gca.2011.03.031

Vona, A., Ryan, A. G., Russell, J. K., & Romano, C. (2016). Models for viscosity and shear localization in bubble-rich magmas. *Earth and Planetary Science Letters*, *449*, 26–38. https://doi.org/10.1016/j.epsl.2016.05.029

Webb, S. L. (2008). Configurational heat capacity of Na_2O–CaO–Al_2O_3–SiO_2 melts. *Chemical Geology*, *256*, 92–101. https://doi.org/10.1016/j.chemgeo.2008.04.003

Whittington, A. G., Hellwig, B. M., Behrens, H., Joachim, B., Stechern, A., & Vetere, F. (2009). The viscosity of hydrous dacitic liquids: Implications for the rheology of evolving silicic magmas. *Bulletin of Volcanology*, *71*, 185–199. https://doi.org/10.1007/s00445-008-0217-y

Whittington, A. G., Richet, P., & Holtz, F. (2000). Water and the viscosity of depolymerized aluminosilicate melts. *Geochimica et Cosmochimica Acta*, *64*, 3725–3736. https://doi.org/10.1016/S0016-7037(00)00448-8

Whittington, A. G., Richet, P., Linard, Y., & Holtz, F. (2001). The viscosity of hydrous Phonolites and Trachytes. *Chemical Geology*, *174*, 209–223. https://doi.org/10.1016/S0009-2541(00)00317-X

Wilke, M. (2005). Fe in magma—An overview. *Annales Geophysicae*, *48*(4–5). https://doi.org/10.4401/ag-3222

Zhang, Y., Xu, Z., & Liu, Y. (2003). Viscosity of hydrous rhyolitic melts inferred from kinetic experiments, and a new viscosity model. *American Mineralogist*, *88*, 1741–1752. https://doi.org/10.2138/am-2003-11-1215

Zheng, Q., Mauro, J. C., Ellison, A. J., Potuzak, M., & Yue, Y. (2011). Universality of the high-temperature viscosity limit of silicate liquids. *Physical Review B: Condensed Matter*, *83*, 212202-1–212202-4. https://doi.org/10.1103/PhysRevB.83.212202

Zheng, Q., Zhang, Y., Montazerian, M., Gulbiten, O., Mauro, J. C., Zanotto, E. D., & Yue, Y. (2019). Understanding glass through differential scanning calorimetry. *Chemical Reviews*, *119*, 7848–7939. https://doi.org/10.1021/acs.chemrev.8b00510